Republic of Iraq

Ministry of Higher Education and Scientific Research

University of Babylon

College of Materials Engineering

Department of Ceramic and Building Materials

Optimization Study of Effect of Partial Stabilized Zirconia Addition Upon Fracture Mechanics of a Hydroxyapatite Using Digital Image Correlation

A Thesis

Submitted to the Council of the College of Materials Engineering / University of Babylon in Partial Fulfillment of the Requirements for the Master degree in Materials Engineering / Ceramic

By

Mariam Ibrahim Oribi Katie

Supervised by

Prof.
Mohsin Abbas Aswad . Ph.D

Prof.
Mohammed A. Ahmed Al-dujaili. Ph.D

2022 A.C **1443 A.H**

بسم الله الرحمن الرحيم

وَيَسْأَلُونَكَ عَنِ الرُّوحِ قُلِ الرُّوحُ مِنْ أَمْرِ رَبِّي وَمَا أُوتِيتُمْ مِنَ الْعِلْمِ إِلَّا قَلِيلًا

﴿٨٥ الإسراء﴾

صدق الله العظيم

The Certificate of Supervisors

We certify that this thesis entitled " ***Optimization Study of Effect of Partial Stabilized Zirconia Addition Upon Fracture Mechanics of a Hydroxyapatite Using Digital Image Correlation*** " was Prepared by (***Mariam Ibrahim oribi***) under our supervision at the Department of ceramic and building Materials / College of Materials Engineering / University of Babylon in partial fulfillment of the requirements for the degree of Master in ceramic.

Signature :

Name : Prof. Mohsin Abbas Aswad , Ph.D.

(supervisor)

Date : / / 2022

Signature :

Name : Prof. Mohammed Assi Al-dujaili , Ph.D.

(supervisor)

Date : / / 2022

Dedication

To my family

For their endless love ,

Support and encouragement

Mariam

2022

Acknowledgments

First of all, profusely all thanks be for ALLAH Lord of all creations who has enabled me to achieve this work.

I would like to express my gratitude to my supervisors, **Dr. Mohsin Abbas Aswad and Dr.Mohammed al-dujaliy** , for their guidance, advice and enthusiastic encouragement throughout this investigation.

I am very grateful to my family and my colleagues especially **Hadeer Sadiq** for her assistance, encouragement and support during the period of preparing this work.

My thanks and gratitude to the Department of Ceramics and Building Materials for providing support and assistance in my work.

My profound appreciation is extended to the members of Ceramic materials laboratories especially **Eng.Haitham, Eng.Ashwaq, Eng.Mahmood, Eng.Khaidaa, Eng.Homam, Eng.Ibtisam, Eng.Khansaa, and Eng.Rehab**.

Additional thanks are to Department of Polymer Engineering and Petrochemical Industries for their support in my work.

I would also like to thank **Dr. Basim Mohysen** for his help in providing the camera used in the experimental work.

Mariam

2022

Abstract

Hydroxyapatite has been extensively explored as a bone replacement material due to its better biocompatibility. Because it closely resembles the bones and teeth, hydroxyapatite is commonly employed as a bioceramic material for human hard tissue implants. Because of its poor mechanical properties especially fracture toughness, synthetic hydroxyapatite is limited used in low-load bearing applications.

In this study, Hydroxyapatite was prepared from bovine femur bone due to economically and environmentally preferable. It was characterized by X-Ray diffraction, particle size analysis, and Fourier transforms infrared Spectrometer.

Hydroxyapatite with (5, 10,15, 20 wt% partial stabilized zirconia) composite fabricated by powder technology method. The specimen was compacted under uniaxial pressing and sintered at 1250 C˚. The mechanical and physical properties of the composite samples were determined.

Single edge notched beam test was used to study the crack opening, crack propagation, and fracture toughness using the powerful optical-numerical method, the digital image correlation technique.

The experimental results showed that (HA/5wt.% PSZ) has the highest value in the physical and mechanical properties than other ratios .where, relative density was 3 g/cm³, porosity (13%), Vickers hardness (3.8GPa), compression strength (98MPa), bending strength (43 MPa) and fracture toughness (1.1 MPa.√m).

Phase transformation of zirconia from tetragonal phase to monoclinic phase was responsible for the toughening mechanism of the

composites as a result of existing the zirconia particles that worked as an obstacle in front of the crack tip.

The genetic algorithm method has been applied to obtain the optimum (density, porosity and critical load) and the best contention of zirconia. The results have shown that the value of best fitness function for density (3.01 g/cm^3) at (3.9 wt.%PSZ), for porosity (6.05%) at (3.3wt.%PSZ) and for critical load (22.2) at (5.1 wt.%PSZ).

List of Figures

List of Contents

List of Tables

List of Abbreviations or Symbols

Abbreviation or Symbol	Meaning
HA	Hydroxyapatite
ZrO_2	Zirconia
PSZ	Partial Stabilized Zirconia
TCP	Tricalcium Phosphates
CZ	Calcium Zirconate
PVA	Polyvinyl Alcohol
XRD	X-Ray Diffraction
SEM	Scanning Electron Microscopy
P.S	Particle Size
FTIR	Fourier transform infrared
COD	Crack opening displacement
CMOD	Crack Mouth Opening displacement
CTOD	Crack Tip Opening displacement
KIC	Fracture toughness
P	Load
Pmax	Maximum (critical) load
LEFM	Liner Elastic fracture mechanics
EDX	Energy dispersive X-ray
ASTM	American Society for Testing Materials
DIC	Digital image Correlation
T	Time
GA	Genetic Algorithms

Chapter one

Introduction

1.1 Overview

Bioceramics is a term used to describe materials used in this medical implant. Depending on the type of bioceramics employed and their interaction with the host tissue, bioceramics are now used in various applications throughout the body [1].

Hydroxyapatite (HA) was studied extensively and is used in bone clinical studies. The growing interest in HA stems from its chemical similarity to the inorganic component of natural bone [2]. HA has been widely used for medical purposes due to its good biocompatibility, very high osseoconductive, and osteoinductive, non-toxic and non-immunogenic [3]. Despite its high biological properties, it exhibits poor mechanical properties, especially fracture toughness, limiting the material's usability and preventing its use in significant load-bearing applications[4].

There are various potential solutions to this problem in the works right now. HA-coated metal implants combine the bioactivity of HA with the toughness and strength of the metal, as well as HA particulate or fibre reinforcing[5].

Due to its superior aesthetics, increased material strength, and good biocompatibility, zirconia has been employed. It stands out among oxide ceramics because of its excellent mechanical qualities, which is a result of the phase transformation toughening mechanism [6].

Failure of engineering materials is one of the most critical research studies of all time due to the cost of undesirable damages and accidents that are resulted from it. Engineers are often required to understand the causes of failures and minimize the probability of failures in the designed components. Cracks are everywhere around us; these cracks, which usually exist, could result from industrial flaws or various environmental conditions during loading. Crack opening displacement and crack propagation are the most critical parameters in fracture mechanics [7].

Fracture mechanics is the discipline that describes how a cracking or defect forms and propagates in the structure under applied loads. Because the cracks can occur anywhere, fracture mechanics has a wide range of applications. Many fields of science and engineering, such as Aerospace Engineering, Geological Engineering, Mechanical Engineering, Civil Engineering Materials and Medical Sciences, have to consider fracture mechanics in their application fields [8].

The samples dimensions of brittle material to be tested is excessively minor to enable extensometers or electromechanical to be used for determining the displacement of the opening crack[9]. The measuring crack opening displacement is difficult and, as values obtain smaller, special equipment is needed, and for a ceramic, SEM, and AFM have been utilized. These methods require precise sample preparation and distinctive care to determine accurate displacement values [10][11]. To circumvent these challenges, a non-contact optical approach called Digital Image Correlation (DIC) can be utilized to calculate a sample's displacement and strain to detect crack propagation and assess crack opening displacement [12].

1.2 Objectives of the Work

The objectives of this study are :

1. Studying the effect of PSZ on mechanical and physical behaviours.

2. Observation of initiation, propagation and opening displacement of a crack in hydroxyapatite and composites by DIC.

3. To find out the optimum weight ratio of PSZ .as well as the optimum values of density, porosity and critical load.

Chapter Two

Theoretical Part and Literature Review

2.1 Introduction

This chapter includes some of the theoretical aspects of the current study, such as Hydroxyapatite, ZrO_2 and their properties, applications, the concept of fracture mechanisms, toughening mechanisms in ceramics, fracture mechanics technique for identifying crack propagation and opening , optimization process, and a literature review on the subject.

2.2 Bioceramics

Ceramics are a type of biomaterial utilized in biomedical devices. This is because of its flexibility to be formed into various shapes and its variable porosity, bioactive properties , and high compressive strength in the body; ceramics are often employed as implant products [13].

Ceramics biomaterials are used to repair tooth and bone defects, fix bone grafts or prostheses in place, repair fractures, and replace damaged tissue. They must be extraordinarily biocompatible, anti-thrombogenic and free of toxins, allergens, carcinogens, and teratogens [14].

There are three types of bioceramics:

(1) bioinert ceramics.

(2) bioactive ceramics.

(3) bioresorbable ceramics.

Bioceramics are produced in a different phases; Polycrystalline (alumina or hydroxyapatite), single crystals (sapphire), glass ceramics (A/W glass-

ceramic), glass (Bioglass), and composites are also possible options (polyethylene-hydroxyapatite)[14].

The high chemical inertia of ceramics, as well as their high compression strength and aesthetic appearance, led to their application in dentistry, particularly in dental crowns. Later on, they were used in orthopaedic applications[15].

2.2.1Hydroxyapatite

Hydroxyapatite is a bioactive material because its Ca/P ratio is near to the Ca/P ratio of bones and teeth. This is made HA a appropriate material for the medical properties as a dense material or as a coating over implants[16]. As a result of these properties, HA is most utilized in biomedical applications, particularly in orthopaedics and dentistry, in addition, the covering material for metallic implants[17].

The apatite family of minerals has a general formula A10(BO4)6X2. In HA, A = Ca, B = P, and X = OH [18]. The OH functional group can be removed from the HA (dehydration). This lead to the decomposition of the HA phase to form α-tricalcium phosphate (α-TCP), (β-tricalcium phosphate β-TCP) and tetracalcium phosphate (TTCP).The decomposition of HA is accompanied by a drop in mechanical properties due to a decrease in densification[19].

The microstructure and sintering ability of HA have a significant impact on its mechanical properties; densely sintered bodies with tiny grains are tougher and stronger than porous bodies with bigger grains[20]**.**

2.2.1.1 The Structure and Composition of Hydroxyapatite

Pure HA [$Ca_{10}(PO_4)_6$ $(OH)_2$] is the most stable calcium phosphate salt at average temperatures, having a stoichiometric apatite phase with a Ca/P molar ratio of 1.67[21]. Two main crystal forms are identified for HA: monoclinic and hexagonal, with the hexagonal form being more stable than the monoclinic [22].

The system has hexagonal rotational symmetry, a reflection plane, and cell parameters of [a=b=9.418 Å , c=6.884 Å, y =120˚] and belongs to the hexagonal space group $P6_3/m$. The HA unit cell is seen in Figure (2.1)[23].

Monoclinic is another form of HA with $P2_1/b$ space group and lattice parameters [a=9.4214, b=2a= c=6.8814 A˚]. The most important difference between monoclinic form and hexagonal form is the OH group orientations. In monoclinic, all OH groups in a column pointed in the one direction and reversed to the next column, but in the hexagonal form, the neighbouring OH group pointed in adverse directions [24].

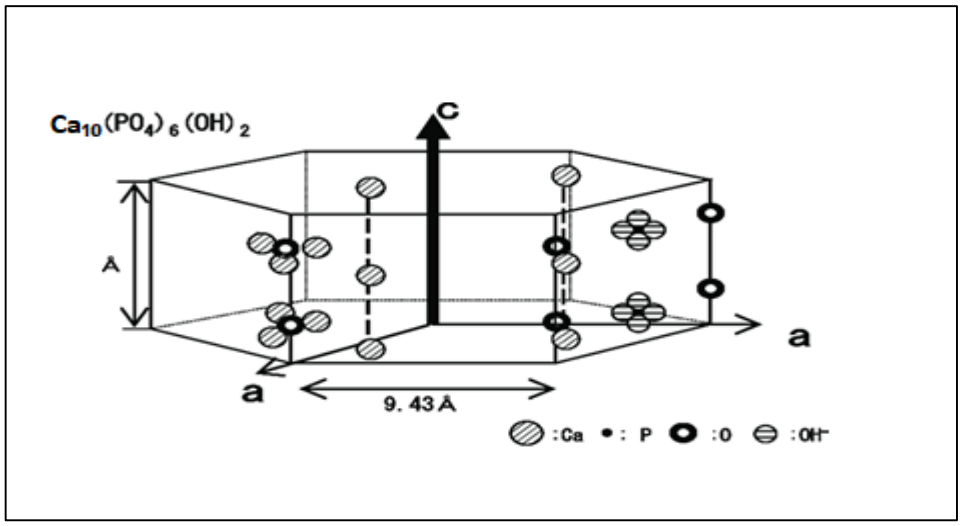

Figure (2.1) Unit Cell Structure of HA [25]**.**

2.2.1.2 Hydroxyapatite Synthesis

Synthetic HA can be made utilizing a variety of procedures, which are divided into three categories: dry, wet, and high-temperature approaches [26]. Moreover, differences in the grain size (small grain size tends to produce more excellent fracture toughness) and composition result from different preparation procedures[27].

Mammalian bone (horse, bovine, and camel), marine or aquatic sources (fish scales and fishbone), shell sources (eggshell, , seashell ,clam, and cockle), plants and algae, also mineral sources can all be used to make hydroxyapatite [28].

2.2.2 Zirconia

Zirconia is a zirconium oxide crystalline form and has a mechanical properties which are very close to metals. Its colour is identical to that of teeth. Furthermore , the melting point is between 2680°C and 2370°C, and zirconia crystals can be structured in three different patterns: monoclinic (M), cubic (C), and tetragonal (T)[29]. A tetragonal form is stable at intermediate temperatures 2370–1170°C and a monoclinic form is stable at lower temperatures[30].

Using pure zirconia ceramics as advanced structural materials are limited due to the spontaneous tetragonal to monoclinic (T→M) phase transformation upon cooling from elaboration temperature to room temperature[31].As shown in figure (2.2).

This martensitic transition results in irreversible damages caused by about 4.5% volume expansion[32]. By adding a stabilizer to a mixture of zirconia polymorphs, stabilized zirconia can be created at room temperature.

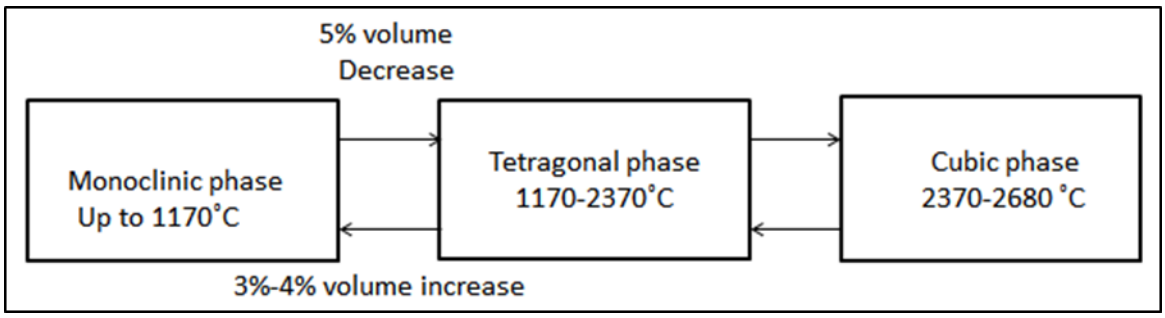

Figure(2.2) Phase transformation of zirconia[31].

Partially stabilized zirconia is multiphase zirconia that has been partially stabilized by adding stabilizing oxides in concentrations lower than those required for the total stability (PSZ)[6] . Figure (2.3) show the phase diagram of Zirconia with Yittria .

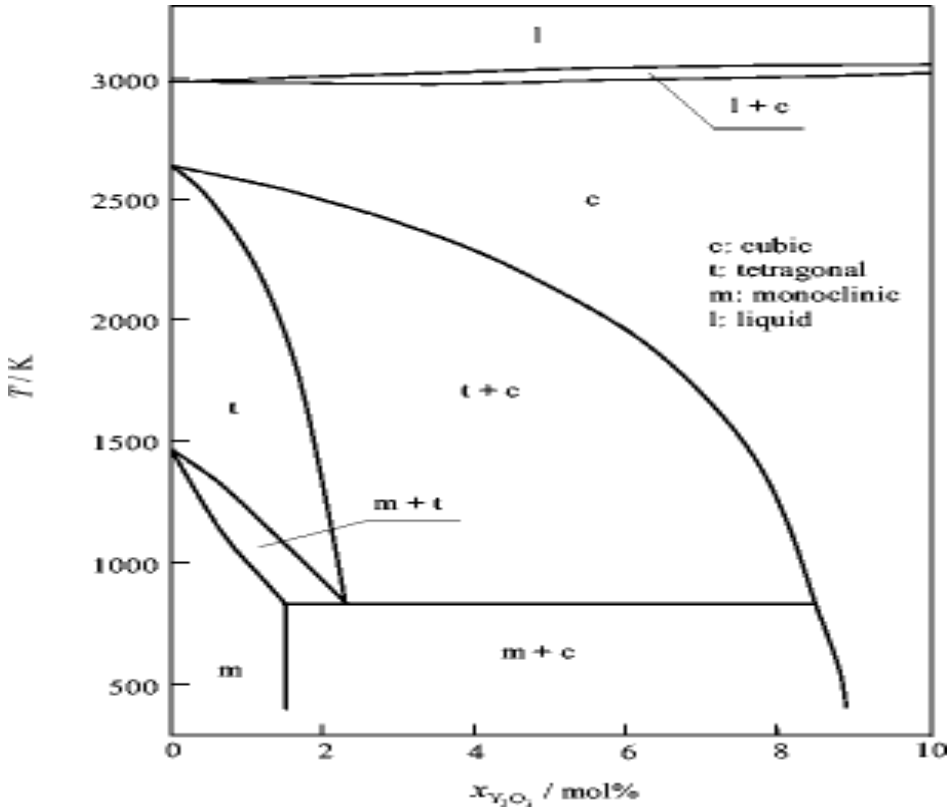

Figure(2.3) Phase diagram of the system ZrO2-Y2O3[33]

2.3 Fracture Mechanics

The phrase fracture mechanics refers to a vital subfield of solid mechanics that aims to discover quantitative correlations among the crack length, material's inherent resistance to crack propagation, and stress at which the crack propagates rapidly enough to induce structural failure [34].

Linear elastic fracture mechanics (LEFM) is a type of fracture mechanics that applies to stress on bodies in the elastic strain area[35].

2.3.1 Linear Elastic Fracture Mechanics

The behaviour of a cracked body under stress is significant in both practical and theoretical terms [36]. In other words, LEFM provides a complete description of the elastic fields surrounding the tip of a single crack, whether static or propagating [37]. LEFM itself is based on the ideas of Griffith, who formulated an energetic criterion for the nucleation or propagation of a crack in a material [38]. The stresses at the tip of the elastic crack must be large enough to induce the crack to fail at the instant of instability. To put it another way, one must suppose that the material contains either a single long crack or a group of tiny cracks that will at least join to form a single big crack capable of causing brittle fractures[39].

The crack tip stress state is characterized by the stress intensity factor K can be utilized for integrate loading conditions (i.e. fracture mode), crack size, and geometry of the cracked body. The critical stress intensity factor KIc is a material property affected by the environment and load rate [40]. It is the critical state in which failure occurs, and it corresponds to the material's resistance to the fracture[41].

2.3.2Griffith Energy Balance

Due to the loads that affect the system, two new surfaces are generated during fracture, and the total energy of the system is either decreased or constant. Griffith proposes an energy balance between potential energy and the work necessary to develop a crack. Under equilibrium conditions, an incremental increase in crack area is given by [42] :

$$\frac{dE}{dA} = \frac{dE_p}{dA} + \frac{dW_s}{dA} = 0 \text{ …….(2.1)}$$

Or

$$-\frac{dE_p}{dA} = \frac{dW_s}{dA} \text{ ……(2.1)}$$

Where E is total energy , E_p is Potential energy from internal strain and external force , and W_s is Work required to create two new surfaces .

This relationship can be illustrated using a cracked plate (as explained in Figure 2.4), which has been subjected to an increase in crack area dA due to crack increment da, resulting in the creation of two new surfaces.

A stress distribution solution from Inglis gives the potential energy in terms of strain energy :

$$E_p = E_{p,0} - \frac{\sigma^2 a^2 B}{E} \text{ …….(2.3)}$$

Where ; Ep,0 is Potential energy of un-cracked plate and E is E-modulus,

The work from surface energy is given by equations:

$$Ws = 4aB\gamma s \text{ …….(2.4)}$$

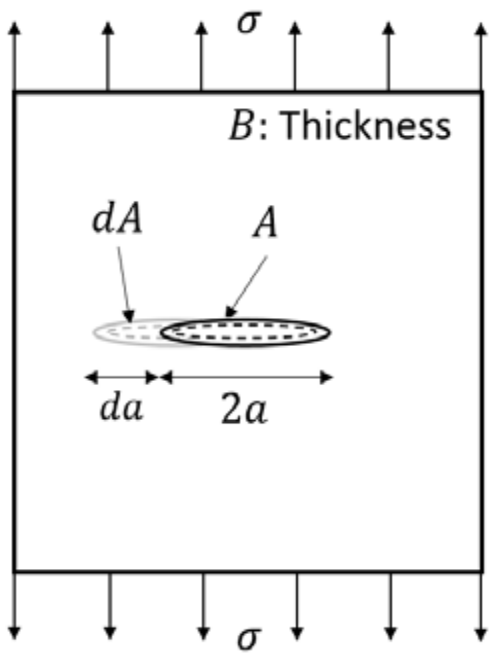

Figure (2.4) Through crack subjected for an increase in crack area.

Where γs is the surface energy of the material. Thus

$$-\frac{dE_p}{dA}=\frac{\pi\sigma^2 a}{E} \quad \text{.....(2.5)}$$

And

$$\frac{dW_s}{dA}=2\gamma_s \text{..... (2.6).}$$

Using equations (2.5) and (2.6) to solve for critical stress σc:

$$\sigma c=\sqrt{\frac{2\gamma_s E}{\pi a}} \text{..... (2.7)}$$

The surface energy γ_s depends on material behaviour and are typically given for brittle materials when the material becomes more ductile; a factor γp that ensure plastic behaviour is introduced.

$$\sigma_c=\sqrt{\frac{2E(\gamma_s+\gamma p)}{2\pi}} \text{.....(2.8)}$$

The following is a generalized expression for any type of energy dissipation:

$$\sigma_c = \sqrt{\frac{2Ewf}{\pi a}} \ldots\ldots\ldots\ldots (2.9)$$

Where, w_f denotes the fracture energy, which can include plastic behaviour depending on the material, and denotes whether or not a fracture occurs due to a specific energy release rate [43].

2.3.3 Deformation Modes at Crack tip

There are three different types of stress fields and displacement modes (As shown in figure 2.5). The displacement of the two crack surfaces as they move directly apart is known as the opening mode "Mode I ". The applied force and displacement v parallel the crack surfaces. The stress intensity factor associated with this mode is KI. The shear or sliding mode "Mode II" happens when the two fracture surfaces are shifted by sliding over one another. The applied load's direction and displacement are parallel to the crack surfaces. The tearing mode "Mode III" arises when the crack surfaces move over each other in a path parallel to the leading edge of the crack [39].

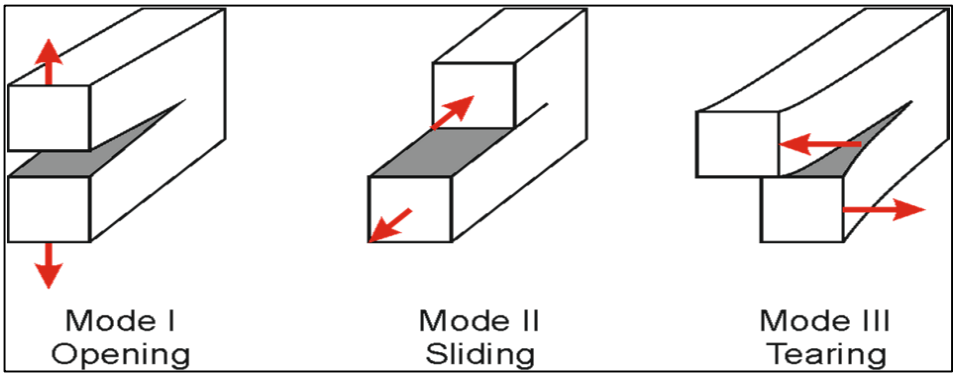

Figure(2.5). Three types of fractures.

2.3.4Fracture Toughness

In a non-corrosive environment, "fracture toughness" refers to a material's resistance to the formation of unstable cracks. This value describes the strength of the stress field near the crack tip when unstable cracking occurs. Although, the plane strain fracture toughness K1c is depending on crack length and thickness. Throughout the literature, the letter I in the subscript is utilized to Mode-induced instability is denoted by the letter I in the subscript. The instability results from the mode I crack propagation with cleavage type fracture (flat fracture surfaces) without shear lip [44].

Fracture toughness is a term that refers to the amount of force required to propagate a preexisting crack. Various flaws are widespread in materials, leading to fracture failure [45].

2.3.5 Stress intensity factor

Irwin demonstrated that a parameter might define the stress field surrounding a sharp crack in a linear elastic material termed the stress intensity factor K. According to him when the value of K exceeds a critical value Kc, fracture ensues. As a result, K is a stress field parameter independent of the material, whereas Kc measures an inherent material property known as fracture toughness [46].

In other words, one of the most critical parameters in the fracture mechanics analysis is the Stress Intensity Factor (SIF). It defines the stress field near the crack tip and provides basic information about how the crack will propagate [47].

The critical value of stress intensity factor in mode I loading measured under plane strain conditions is known as a plane strain fracture toughness, denoted KIC[48].

K is a quantity that provides the amount of elastic crack tip stress field. For an infinite plate with a crack under tensile stress, the stress components are expressed in equations (2. 10), (2. 11), and (2.12):

$$\sigma_x = \frac{KI}{\sqrt{2\pi r}}(1- \sin(\frac{\theta}{2})\ \sin(\frac{3\theta}{2}))\ \cos\frac{\theta}{2} \quad \text{……. (2.10)}$$

$$\sigma_y = \frac{KI}{\sqrt{2\pi r}}(1+ \sin(\frac{\theta}{2})\ \sin(\frac{3\theta}{2}))\ \cos\frac{\theta}{2} \quad \text{…….. (2.11)}$$

$$\tau_{xy} = \frac{KI}{\sqrt{2\pi r}}\cos(\frac{\theta}{2})\ \sin(\frac{3\theta}{2})\ \cos(\frac{3\theta}{2}) \quad \text{…….. (2.12)}$$

Where (θ, r) denote polar coordinates at the crack tip, and KI denotes the intensity factor.

According to the equations, the stress components are consisting of the stress intensity factor K_I and the geometry factor. Equation (2.13) shows how to express the stress intensity factor K_I:

$$K_I = \sigma\sqrt{\pi a} \quad \text{…….. (2. 13)}$$

Where a is the central crack's half crack length, and σ is the applied stress[49].

2.3.6Crack Opening Displacement (COD)

COD, originally termed "crack opening displacement", is linked to LEFM through the recognition that in any real material, there is a "plastic zone" around the crack tip which necessitates modification of the purely linear model [50][51].

Crack opening displacement (COD) is a parameter describing the near-tip crack profile and predicting the fracture. It is defined as a relative opening movement of the upper and lower crack flanks [41].

When the displacement is measured near the crack mouth, the term "Crack Mouth Opening Displacement (CMOD) " is used, and when the displacement is measured at the intersection of a 90° vertex with the crack edges the term " Crack Tip Opening Displacement (CTOD) " is used [52]. see Figure (2.6)

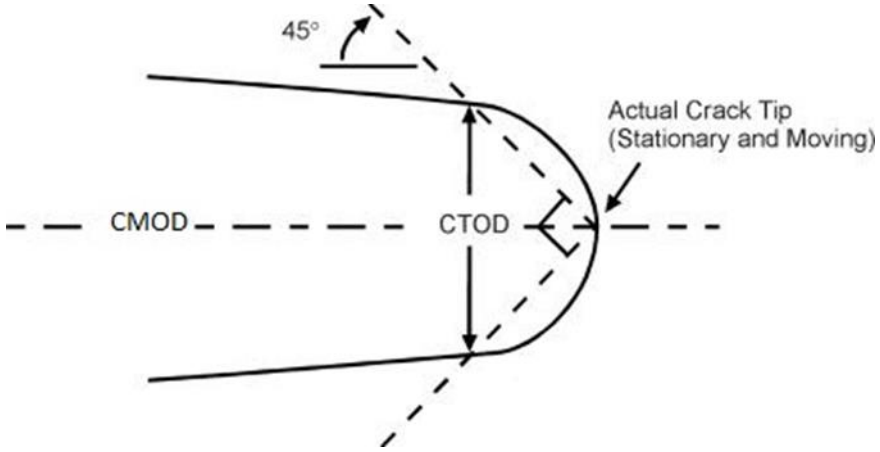

Figure (2.6) Show CTOD and CMOD [53]**.**

2.3.7 Crack Propagation

The crack propagation can be thought of as the following rupture of the bonds that hold the atoms together; this is according to the general analysis of fracture in the solid body. The material's structure can be considered a regular arrangement of the point masses (atoms) spaced by the same equilibrium spacing. The atomic bonds can be regarded as springs, both linear and nonlinear (cohesive bonds), with a bond stiffness [54].

When a material is subjected to an external load, the atoms are moved from their original equilibrium position, straining on their bonds at the atomic level. The external load on the material must translate to an acting atomic-level force; this is larger than the cohesive force binding the atoms for a bond to be severed and an atom to be permanently displaced

from its equilibrium position. The force must also complete a minimum amount of work equal to the bond energy.

Figure (2.7) (a) shows an idealized interaction between two atoms as a function of their separation distance along with an atomistic view of crack extension shown in figure (2.7) (b) and shows the Crack occurs when the local force experienced by atoms due to the external loading is enough to drive a cascade of bond breaking [42].

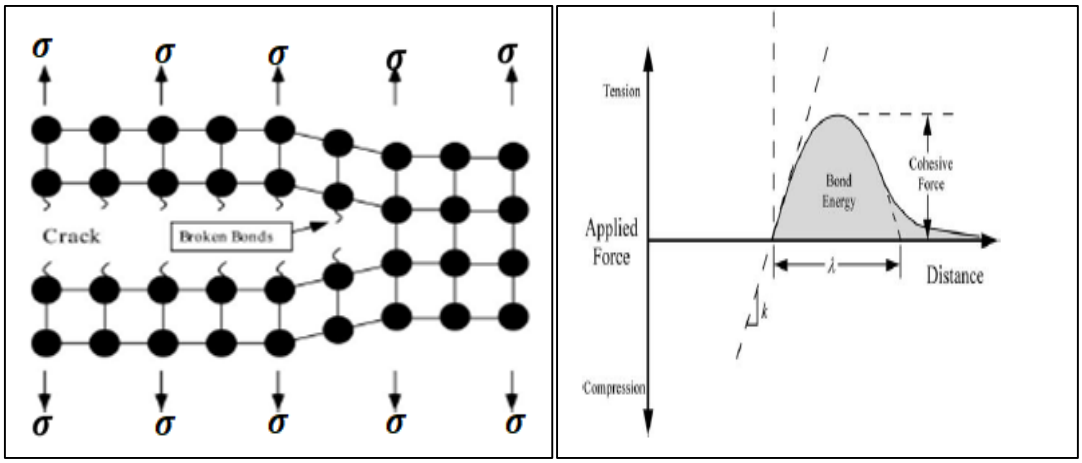

Figure (2. 7) (a) A plot of potential energy and force magnitude as a function of atom separation distance, (b) An atomistic view of crack extension via bond breaking [42].

2.3.8Toughness Measurement

Many methods are currently utilized to measure the fracture toughness (KI) of ceramic materials [55]; such as double cantilever beam(DCB), surface crack in flexure (SCF), indentation fracture (IF), single-edge V-notched beam (SEVNB), single-edge precracked beam (SEPB), single-edge notched beam(SENB), and chevron notch (CN) [56].

2.3.9 Toughening Mechanism

Dislocation movement in ceramics with strong bonds is challenging due to directional properties and the intrinsically rigid bond network; as a result, movement necessitates bond breaking and remaking, as well as distorted bond angles. As a result, any uniform deformation without localized fracture is impossible, and cracks in ceramics are rather easy to form[57]. Toughness has been thought to be the material's ability to dissipate deformation energy without the propagation of a crack [58]. Figure (2.8) display the toughening mechanisms.

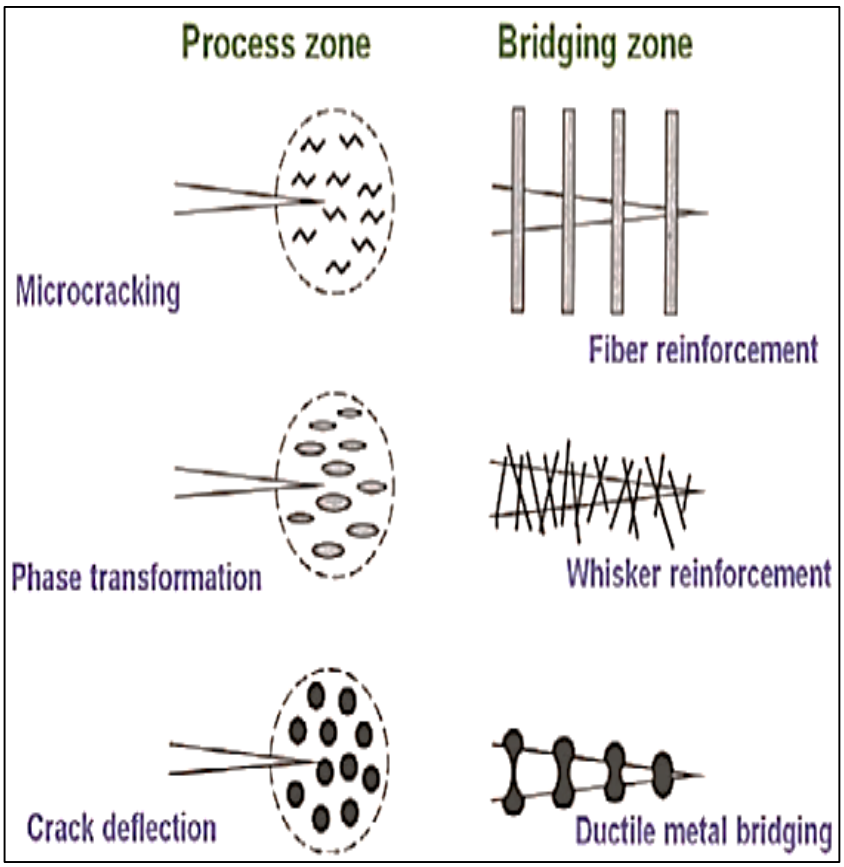

Figure (2.8) Toughening Mechanism[57].

2.3.9.1 Process Zone

Extrinsic toughening processes that limit apparent applied stress intensity at the crack tip to the material's intrinsic toughness are known as process zone mechanisms [59].

a) Crack deflection and meandering

Residual stresses, Fracture resistant second phase particles,and Grain boundaries are examples of how cracks might deviate from their planned path. The crack driving force, or crack tip stress intensity factor (K), is lowered when the crack plane is reoriented from average to the applied tension, resulting in enhanced Toughness. The nature of the crack deflection and particulate phase that generates it has a significant effect on the toughness increase feasible with this method. The volume fraction and shape of the particles affect the toughening obtained from randomly oriented and deflected particles. Because they influence the twist angle, rod-shaped particles with a large aspect ratio contribute significantly toughening. Toughening saturates with relatively low second phase particle volume fractions, which is a feature of this mechanism. Another critical characteristic of this mechanism that is temperature and the particle size independent [59].

b) Transformation Mechanism

One way to enhance the crack propagation resistance in the materials is transformation toughening. The increase in Toughness is due to the martensitic change of the microstructure to a metastable phase. This returns to a stable state when the pressure or temperature from the environment is applied. A typical ceramic crack travel through the material with no restriction, resulting in brittle fracture. the strain field around the changed reinforcement prevents cracks as much as possible from doing so. The fracture toughness of the transformation hardened zirconia is 3–6 times that of conventional zirconia and most other ceramics.

However, between ambient temperature and 950 °C, zirconia has a monoclinic crystal structure. Zirconia transforms into a tetragonal crystal structure at temperatures above 950°C. There is more than 3% shrinkage

during the heating process, and the cooling process results in an equivalent expansion. The zirconia converts from a tetragonal to a cubic structure at a much higher temperature. During cooling, the microstructure consisting of tetragonal zirconia precipitates in cubic zirconia grains can be formed with the proper chemical additives and heat treatments (PSZ). The tetragonal material normally converts to the monoclinic form during cooling, accompanied by an expansion[60].

c) Microcrack toughening

Microcracking results in the crack shielding by locally reducing at the elastic modulus and spreading the applied stress over many cracks rather than one primary crack. A ductile zone results in the crack shielding by allowing plastic deformation around the crack tip[61].

2.4 Digital Imaging Correlation

The Digital Imaging Correlation (DIC) has the potential to be the best tool for analyzing crack propagation and material deformation in real-world applications; this is because it is a cheap, simple, and exact solution [62].

DIC has significant benefits such as a simple experimental setup and easy implementation, non-contact full-field measurements, and a broad range of applicability with the variable resolution. Two-Dimensional measurements are becoming more popular. The full-field plane displacement and strain measurements of the planar objects utilizing (2D-DIC) to use an optical imaging lens and a single digital camera were commonly applied in the field of experimental mechanics. The imaging lens optical axis should be perpendicular to the planar test sample in 2D_DIC measurements. To create a digital image, On the camera's sensor plane, the speckle pattern on the test planar specimen surface is imaged.

Also, using well-known subset-based cross-correlation algorithms to track the same points of interest from (reference)and (deformed) images taken at different levels of deformation, the researchers were able to identify the same points of interest. The full-field motions in the sensor (image) plane be then can convert into the desired full-field displacement, and the strain results on the corresponding object [63]

2.4.1Basic principle

DIC is used to compare digital images of a component or test piece at various degrees of deformation. The system can track blocks of pixels and Deformation vector fields, as well as strain maps in 2D and 3D, to measure surface displacement and build up a full field[62].

However, DIC Stages in 2D gives [63] :

a) Displacements are immediately recognized from the digital image of an object's (sample) surface in two-dimensional digital image correlation.

- The images on the object's surface are recorded and saved as digital images on a computer, one before and one after deformation. These photos are compared to find displacements via looking for a matching point from one to the following.
- To perform the matching procedure, it contains an area with many pixel points. This area, referred to as a subset, has a distinct light intensity (gray level) distribution inside it.
- By looking for an area with the same light intensity distribution as the subset on the picture before deformation, It is possible to determine the displacement of the subset on the image before deformation in the picture after distortion. Once the location of this

subset in the deformed image has been located, the displacement may be calculated [63][44][44][44][51].

- The object's surface must have a feature that permits the subset to be matched to finish this operation. A random pattern must be created artificially if no feature can be detected on the object's surface [63][44][44][44][51].

Based on the above fundamental principle, many functions match the subset from one image to another. One is the magnitude of the difference in intensity values :

$$R(x, y, x^*, y^*) = \sum F(x, y) - G(x^*, y^*) \ldots\ldots\ldots\ldots (2.14)$$

Another is the normalized cross-correlation, which is calculated as follows:

$$C(x, y, x*, y*) = \frac{\sum F(x,y)\, G(x*,y*)}{\sqrt{\sum F(x,y)^2 \sum G(x*,y*)^2}}*) \ldots\ldots\ldots (2.15)$$

Where ; (x,y) and (x*,y*) are the coordinates of a point on the subset before and after deformation. F(x, y) and G(x*, y*) is the grey levels inside the subset of undeformed and deformed pictures, respectively. The sum of the values within the subset is represented by the symbol for summation. After deformation, the coordinates (x*,y*) are related to the coordinates (x,y) before deformation. After deformation, the optimal set of coordinates (x*,y*) that minimize R(x,y,x*,y*) or maximize C(x,y,x*,y*) was used to find out displacement components. The except for Eqs. (2.14) and (2.15) any function can be employed; therefore, the normalized cross-correlation [Eq. (2.14)] is extensively utilized in the digital image correlation for matching the subset [64].

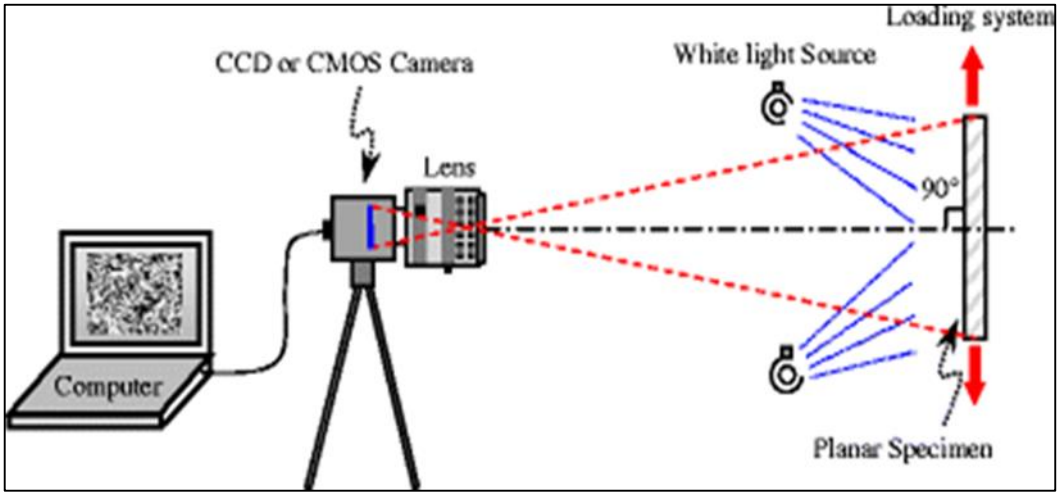

Figure (2.9) The setup of digital image correlation [63].

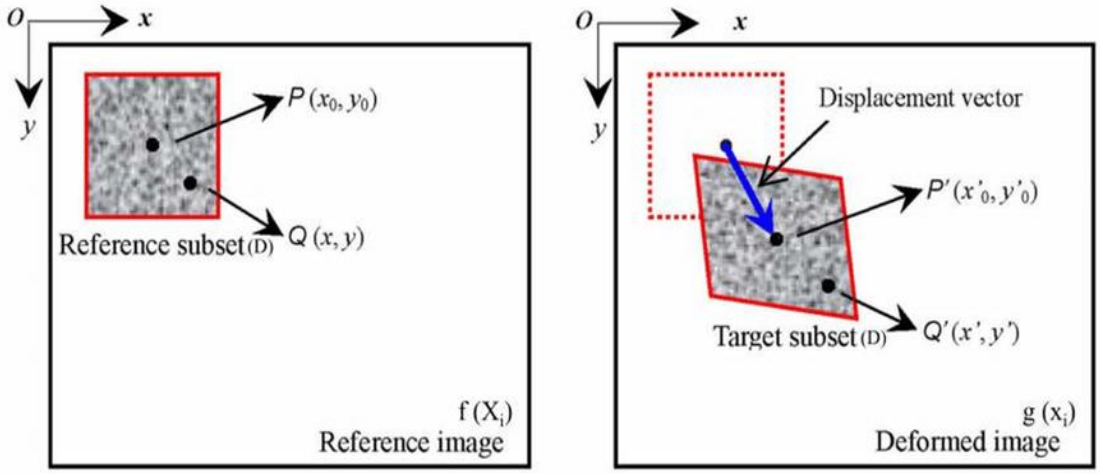

Figure (2.10) The matching between subset before and after deformation [65].

2.4.2 Advantage and Dis Advantage of DIC

Table (2.1) shows the summary of the advantage and disadvantages of DIC [66].

Table (2.1) Advantage and disadvantages of DIC

Advantage	**Disadvantage**
• Full-field displacement/strain measuring • For specimens of any size and material • Determination of stress concentrators and strain gradients • It can be used for both small and large deformations • It can be used in vivo	• Techniques are less exact and accurate than others. • A careful optimization for the unique application is required. • It's not real-time. • Optical access to the specimen is required • Surface preparation is required

2.5 Literature review

2.5.1 Hydroxyapatite preparation

Hilmi Isom, et al .(2011). Described the method for extracting hydroxyapatite from animal (bovine) bones. A calcination process completed the defatting process at 900˚C to produce bovine HA in the bulk form from bovine bone. X-ray diffraction XRD and Fourier transformed infrared FTIR spectroscopy characterize the calcined products. The particles in the HA phase is highly crystalline and irregular in shape (particle size 45 μm) [67].

Jojor Lamsihar Manalu ,et al. (2015). Studied preparation of HA from bovine bone by heated at different temperatures from 700Cº to 1000Cº . The final product was characterized by Xray, EDX, and FTIR in which the phase, purity and crystallinity of the calcined HA were analyzed to a different temperature.The desired quality was demonstrated by the natural HA obtained by calcination at 850 °C. In addition, the formation of microstructured HA 0.4 μm at 700 ° C was revealed by SEM results, and crystal agglomeration with an increase in calcination temperature was observed [68].

2.5.2 Toughening of Hydroxyapatite

Sakakura.S, et al .(2003). Studied the toughening of hydroxyapatite and improved its properties by using silver particle via three methods (traditional sintering, hot isostatic pressing, and their combination). Hydroxyapatite was prepared with silver particle as a composite material After that, several tests were performed through which the highest density, and highest hardness were reached by the hot-isostatic pressing method with a silver volume fraction of 30%. Furthermore, this is enhanced HA/Ag composite technique produced a tough material with high fracture resistance. The composite's excellent fracture behaviour was investigated by determining its load-displacement dependency, as well as its R-curve behaviour. According to the microscope results, the increased toughening is attributable to a crack bridge mechanism, in which the crack bridging toughening capacity is directly proportional to the increased interfacial bonding between Ag inclusions and the HA [69].

R. E. Clegg , et al . (2004) Described adding ductile platinum particles to a HA matrix to improve fracture toughness. The Vickers indentation technique was used to determine the composite's fracture toughness and the effect of the volume percentage of platinum particles on the fracture

toughness. Dried ammonium hexachloro-platinate was combined with HA powder, and The mixture was crushed to 10MPa in a die to generate discs with a diameter of 12.4 mm and a thickness of 2 mm. Then, the discs heated to 456°C to dissolve the ammonium hexachloroplatinate (ACP) and produce a thin homogeneous dispersion of platinum particles throughout the HA The material's fracture toughness at a given volume fraction appeared to rise marginally as the sintering temperature increased. The discs were re-pressed to 80MPa and sintered for four hours at 1250°C, 1300°C, and 1350°C. The length of cracks coming from the Vickers hardness impressions was used to calculate fracture toughness. The addition of platinum particles to the ceramic matrix boosted fracture toughness by up to two times that of the untoughened counterpart [70].

Erkmen. Z. E., et al. (2007).Studied the effect of adding zirconia (PSZ) to hydroxyapatite (Enamel derived from human teeth and commercial HA) as a composite material. A temperature range between (1000 C˚-1300 C˚) was used. The ratio of zirconia is 5%,10%. HA-PSZ composite was characterized by using XRD, SEM and particle size. Density, hardness and compressive strength were calculated. The particle size for EHA was 1.5µm, CHA 0.5 µm and PSZ 0.7. The best density was obtained for EHA and CHA at (5%PSZ,1200 C˚) and the best microhardness at 1300 C˚[71].

Leong, C. H., et al . (2014). Studied the effect of adding zirconia (PSZ) on the dissociation of hydroxyapatite and the relationship between mechanical properties and microstructure were studied. Wet ball milling prepared a HA/YSZ nanocomposite as a composite material. Various amounts of 3YSZ (0, 0.5, 1, and 7 wt%) at a temperature of 1250 C˚ by Two sintering methods (Gas pressure and traditional sintering) were used. The study found an effect of zirconia on phase stability morphology, density and hardness; the study, when compared to conventional sintering, gas pressure

sintering results in larger grain size creation. Relative density and microhardness were deteriorated due to particularly severe HA decomposition and the existence of porosity in (HA/ 7YSZwt%). In this paper, (HA/0.5 YSZ wt%) displayed the best microstructure with the best relative density and microhardness [72].

Aguirre, T. G., et al .(2019). The study tried to increase the fracture toughness and flexural strength of HA composites fabricated by adding boron nitride nanoplatelets (BNNP) as reinforcement. So, to produce fine grain structure, spark plasma sintering was used. (0.5 wt% and 1 wt% of BNNP) were addied to facilitated grain size refinement. The flexural strength and fracture toughness were (79.79 MPa) , (2.3 MPam1/2) respectively , of the BNNP reinforced HA composites were higher than previously published values (1.0 MPam1/2). In four -point bending tests, researchers employed the Single Edge V-Notch Beam (SEVNB) method to calculate KIC [73].

2.5.3 Investigation fracture behaviour by DIC.

Pittari, J., et al . (2015). This study utilized a four-point bend, a chevron-notch testing method, to analyze the quasi-static fracture toughness (KIc) of pressureless sintered and reaction-bonded ceramics. The sample geometry complies with ASTM C1421 Testing Standard Configuration A. An electro-mechanical universal testing machine was used to conduct the tests. The crack mouth opening displacement was recorded using (DIC) to validate steady crack nucleation and growth. This is because silicon phase is present, which possesses a quasi-ductile fracture behaviour, the reaction-bonded composite had a more excellent KIc value than the pressureless sintered ceramic, which could be advantageous for the applications requiring ceramics that are less susceptible to brittle fracture[74].

Mohammed M. Hussien , et al. (2017) Fracture behaviour of HA samples were explored (crack observation, initiation, opening, and propagation). This study looked at a single edge notched beam in a three-point bending test. At a critical bending strain of around 10 N, the critical CMOD and CTOD were 40 and 17 m, respectively. Critical time for nucleation was 210sec, and fracture toughness was 0.7 MPa √m. The DIC approach was proven to be a good and exact instrument for measuring fractures such as crack opening and crack length[75].

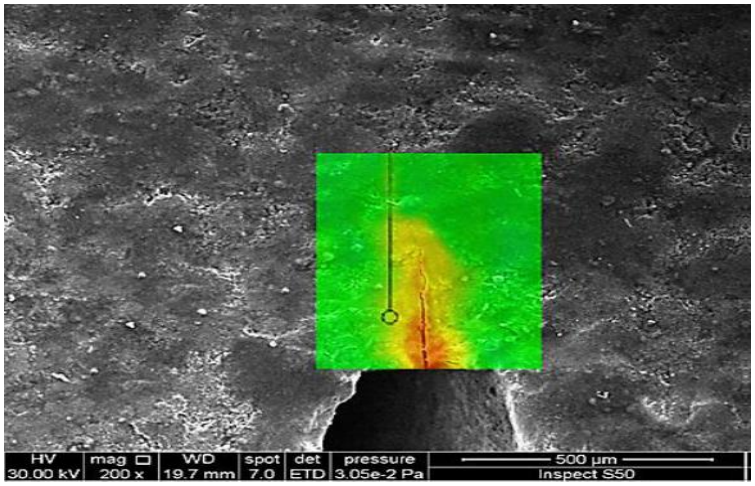

Figure (2.11). Correlation between SEM and DIC of HA specimen after bending test[75].

Azhar abd Selman, et al. incorporated the silver particles into a hydroxyapatite matrix to improve the fracture toughness. the composite material has been fabricated by powder technology method, specimen compacted under uniaxial pressing and a conventional powder sintering. SENB test was used for the determination of opening mode I fracture toughness, KIC, and using digital image correlation(DIC) method, which was a powerful optical-numerical method developed to determine crack propagation and crack opening displacement, COD fields. The results showed that silver has a positive effect on the physical and mechanical properties of hydroxyapatite. SEM results of the toughening mechanism

indicated that crack bridging, crack deflection and subsequent plastic work of silver were responsible for the toughening[76].

Hadeer S. Abd Ali ,et al. (2021). Investigated the mechanical behaviour (i.e. crack opening displacement and fracture toughness) of bioglass-ceramic was studied after adding (3, 5 wt%) zirconia as a reinforcement. However, a three-point bending technique was used to determine fracture toughness. DIC technique used to visualize the crack initiation, measure the crack propagation of the bioactive glass-ceramic/zirconia composite and determine the COD at the tip and mouth of the crack. Critical load for the pure bioactive and bioactive glass /(3,5wt%) zirconia were (11,15, 22 N). The addition of zirconia particles increased the toughness of composite bioceramics by causing fracture branching and crack deflection (see figure) (2.13)[77].

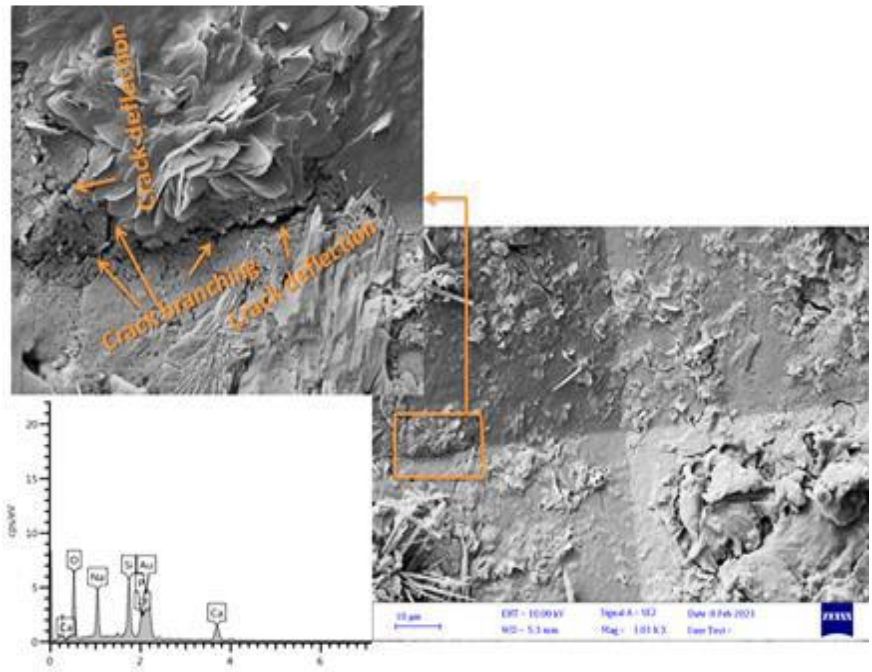

Figure(2.12). Propagation of cracks in a BGC/5 % ZrO_2 sample[77].

2.5.4 Studies Related to Genetic Algorithm Optimization

Hassanien Nadhim, et al . (2016). Applied the genetic algorithm GA approach to determine the optimum compressive strength of hydroxyapatite/ β-TCP composite. The input parameters taken were the ratio of brushite and porosity. While the output parameter taken were the compressive strength. MINITAB software was used to determine the regression equation. The results revealed that the optimum compressive strength was 54.67 MPa [78].

Raghda Ibrahim Abdalwahad, et al. (2018). Were used the GA approach to determine the optimum density and porosity of HA/ bioactive glass-ceramics composite. The input parameters taken were the ratio of bioactive glass ceramics, while the output parameter taken were the porosity and density. MINITAB software was used to determine the regression equation. The best porosity result was 12.34 and 2.61587 for the density [79].

Authors / Year	Ref	Summery
Hilmi, I., Rinastiti, M., & Herliansyah, M. K. (2011, November)	[67]	HA was Extracting from animal (bovine) bones calcination at 900˚C and characterization by XRD and FTIR.
Jojor Lamsihar Manalu (2015)	[68]	HA was Extracting from animal (bovine) bones at temperature (700 - 1000)˚C .final powder characterization by XRD, EDX and FTIR.
Asmus, S. M. F., Sakakura, S., & Pezzotti, G. (2003)	[69]	HA was toughening HA by Silver particles by three methods that improved their properties. The higher interfacial bonding between silver inclusions and the HA matrix is significantly connected with crack bridging toughening capacity.
R. E. Clegg and G.D .Paterson(2004).	[70]	HA was Toughening by ductile platinum particles lead to improve fracture toughness. Platinum particles added to the ceramic matrix increased fracture toughness by up to double than the untoughened counterpart.
Erkmen, Z. E., Genc, Y., & Oktar, F. N. (2007)	[71]	Comparison and Toughening (EHA and CHA) by zirconia (3PSZ) as a composite material at temperature range (1000-1300) ˚C. HA-PSZ composite was characterized by using XRD, SEM and particle size.

Leong, C. H., Muchtar, A., Tan, C. Y., Razali, M., & Amat, N. F. (2014)	[72]	HA was Toughening by addition (3YSZ) at 1250˚C, using two sintering methods. Compared to traditional sintering, gas pressure sintering results in larger grain size formation. The optimum microstructure with the highest relative density and hardness was HA/0.5 wt % YSZ.
Aguirre, T. G., Cramer, C. L., Torres, V. P., Hammann, T. J., Holland, T. B., & Ma, K. (2019).	[73]	Spark plasma sintering was used to enhance the KIC and flexural strength of HA composites , reinforcement is boron nitride nanoplatelets (BNNP).
Pittari, J., & Subhash, G. (2015)	[74]	Study (CMOD) was recorded using the (DIC) technique to validate controlled crack nucleation and growth, by four-point bend, to study the quasi-static (KIC) of pressure less-sintered and reaction-bonded ceramics.
Mohammed M. Hussien, et al (2017)	[75]	Study Fracture behaviour of HA, Measurement (KIc) and COD with DIC by the single-edge notched beam in a three-point bending test.
Azhar abd Selman	[76]	Study Fracture behaviour of HA and HA/Ag composite , Measurement (KIc) and COD with DIC by the single-edge notched beam in a three-point bending test.
Hadeer S. Abd Ali (2021)	[77]	Study mechanical behaviour of bioactive glass-ceramic after

		toughening with zirconia.
Hassanien Nadhim (2016).	[78]	Determine the optimum compressive strength of hydroxyapatite/ β-TCP composite by GA method .
Raghda Ibrahim Abdalwahad (2018)	[79]	Determine the optimum density and porosity of HA/ bioactive glass-ceramics composite by the GA method.

Chapter Three

Optimization Method

3.1 Introduction

Genetic Algorithms (GA) is a stochastic global numerical technique modelled after spontaneous biological evolution. The survival of the fittest principle was used by GAs to make (hopefully) better and good approximations to the solution from a population of the possible solutions. That each generation develops different group of approximations via selecting individuals based on their fitness levels in the problem region and breeding them utilizing natural genetics operators. This technique, like biological adaptation, develops groups of individuals which are more suited to their surroundings than the ones from which they came [80].

GA mimic the processes necessary for evolution to occur in the natural world. It's still a work in progress to determine which biological processes are critical for evolution and which ones have little or no role, but the foundations are apparent [81]. However, the GA was employed for a broad range of optimization issues such as; graphical colouring, recognizing patterns, discrete systems, continuous systems, financial market and multi-objective engineering optimization [82]. When employing GA to optimization, there are several main benefits:-

- Adaptability: Due to its evolutionary character, the GA has few mathematical requirements and searches for solutions without considering the problem's unique inner workings or constraints.
- Robustness: The GA's usage of evaluation operators allows it to perform very well in global search.

- Flexibility: The GA has a lot of flexibility in combining it with domain-dependent heuristics to achieve efficient implantation for a given problem. [83] .

3.2Basic components common to almost all genetic algorithms:

The necessary steps of the GA are shown in Figure (3.1). In a brief, the GA's first step is to create an initial population of individuals, with the individuals representing a possible solution. The next step is to use the fitness function to assess the individuals. There are three operators of GA (mutation , crossover and reproduction) are then utilized to produce new population of points based on the existing population [84].

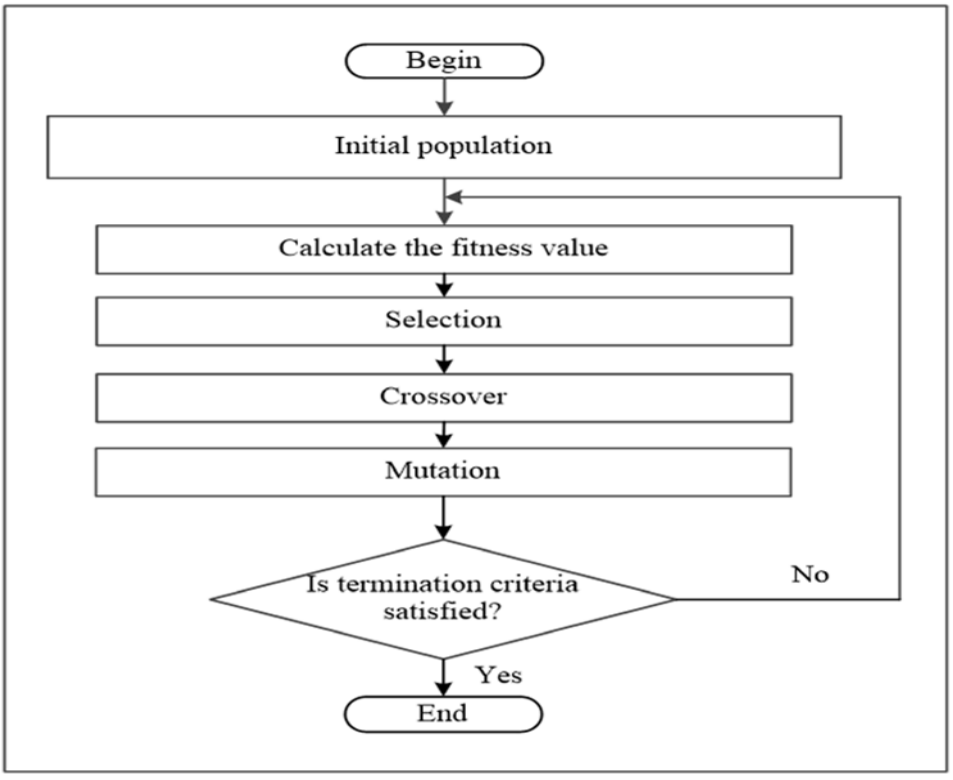

Figure (3.1) Essential steps in the genetic algorithm [85].

3.2.1 Initial Population

The GA method begins with a completely random population. To boost the diversity of this population, a Gaussian random distribution can be used. This population contains many solutions, each representing the

individual's chromosomes. The genes are represented by a set of variables on each chromosome. The principal objective of the initialization process is to distribute the solutions as evenly as possible across the search area to boost population diversity and improve the chances of identifying attractive regions[86].

3.2.2 Fitness Function

To create a search process, GAs use nature's survival of the fittest concept. As a result, GAs are well-suited to resolving maximizing problems; by applying the appropriate transformation, maximization issues are often turned into maximization problems. In most cases, the objective function was used to derive the fitness function F(i), which is subsequently utilized in following genetic operations. In biology, fitness is a quality parameter that measures chromosome reproductive efficiency. Fitness function was being used in the genetic algorithms to assign reproductive qualities to the individuals in the population, serving as a measure of goodness that should be maximized. Individuals fitness with high values will have a better chance of getting selected for additional testing. A non-negative fitness function is required for some genetic approaches but not others. The fitness function and the objective function F(i) = O, are the same in maximizing problems (i). It's required to convert the underlying natural objective function to the fitness function form concerns for the minimization in order to obtain non-negative outcomes over all scenarios and to reflect the proportional fitness of the individual strings. There are many different transformations to choose from. The following are two fitness mapping are used. This transformation does not change the location of the minimum, but it does change the problem from minimization to maximization[87].

$$F(X) = 1/(1 + f(x)).....(3.1)$$

The fitness value F(i) can be obtained using an alternative function to convert the objective function.

$$F(i) = V - \frac{O(i)P}{\sum_{i=1}^{P} O(i)} \ldots\ldots\ldots (3.2)$$

where O(i) is the individual's objective function value, P is the population size, and V is a critical factor in guaranteeing that the fitness value is not negative.

The fitness value is zero for the highest value of the objective function, while the value of V employed in this experiment is the higher value of the second term of Equ (3.2). This transformation doesn't affect the location of the solution, but it does convert a minimization problem to a maximization problem. String fitness refers to a string's fitness function [87].

3.2.3 Selection

The fundamental concept of Selection is that it should be linked to the fitness, As well as the roulette-wheel approach was the initial scheme for implementing it. It utilizes a possibility distribution for Selection in which the selection possibility of a given string is proportional to its fitness[88]. However, there are many types of selection methods used in GA, including (Truncation selection, Tournament selection , Rank-based fitness assignment, Local Selection, and Roulette wheel selection) [89].

3.3 Genetic Operators.

3.3.1 Recombination (Crossover).

An essential operator for adding more chromosomes in the GA is crossover. Crossover, like its natural counterpart, produces new people with genetic material from both parents[80]. Crossover comes in three

varieties One point crossover, Multipoint crossover and Uniform crossover [90].

- One point crossover

A single point called the crossover point is selected at random in this type. The data from the first parent is directly copied before this point, and the data from the second parent is copied to make new offspring. Figure depicts this (3.2).

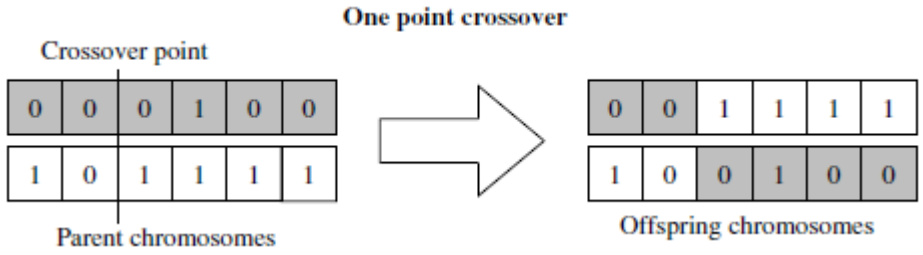

Figure (3.2) One point crossover[91].

- Two-point crossover

The initial part of the offspring is duplicated from the first parent to the first crossover point, with two points chosen at random in the parents. The portion between the first and second crossover points comes from the second parent, whereas the reminder comes from the first. The diagram illustrates this (3.3).

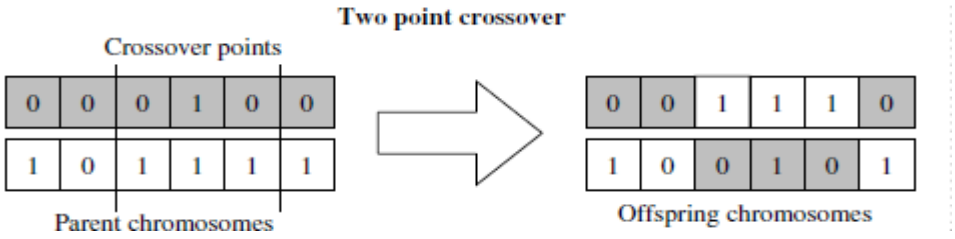

Figure (3.3) Two point crossover[91].

- Uniform crossover

In this sort of crossover, the offspring is made up of genes chosen at random from the parents. Figure (3.4) depicted Uniform crossover.

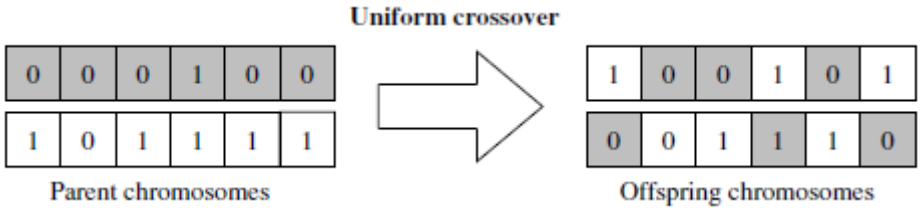

Figure (3.4) The Uniform crossover [91].

3.3.2 Mutation

The crossover operator is the primary means of generating new strings with higher the fitness values for future generations. With a certain modest mutation probability Pm, the mutation operator is applied to the new strings [92]. It usually has a value between 0.001 and0.01, affecting chromosomal elements. The mutation is commonly thought of as a background operator that guarantees that the likelihood of searching any given string never reaches zero. As well as offering a safety net for recovering excellent genetic material that has been lost due to selection and crossover [93]. There are two different types of mutation methods [94].

- Single point mutation

It entails altering the value of single gen in order to create a new chromosome.

- Multipoint mutation

It entails altering the multi-gen values in order to produce a new chromosome.

The following are the objectives of mutation [92] **:**

- to create a string (design point) in the immediate vicinity of the existing string, completing a local search around the current solution
- to protect critical genetic material from being lost prematurely at a specific location
- to preserve population diversity.

Chapter Four

Experimental Work

4.1 Introduction

This chapter describes how to make HA powder and HA/PSZ composite, prepare specimens for the digital image correlation, then study crack propagation, COD, and fracture toughness using the DIC technique.

4.2 Preparation of Hydroxyapatite Powder

As a starting biosource material, bovine femur bone was selected. The spongy bones have been removed, and the bones have been deflated. All of the meat and fat components, and the bone marrow, were separated. The clean bone was used with a gas flame under direct ignition at a temperature of 700 ºC for 7h, and organic sections were charred. This method generates some carbonises due to the combustion of organic ingredients. Inside an air furnace, the black powder (bone ash) was deposited. At 1000 ºC for 3 h to extract the residual carbon, then cooled within the furnace. Following this procedure, the black ash is turned into a white powder. The scale of the powder particles was between only a few millimetres. To reduce the particle size, it was processed utilising a system of planetary ball mills. It was also constituted of an alumina jar and balls (SFM 1Desk-top planetary ball miller); this process was used after heat treatment to produce very fine particles. 30 g powder to 300 g ball was the feed ratio (1 to 10 weight ratio). The speed of milling was set to 300rpm, and the milling time was 3 h. Figure (4.1) explains preparing HA powder from bovine bones.

Figure (4.1) HA powder after calcination.

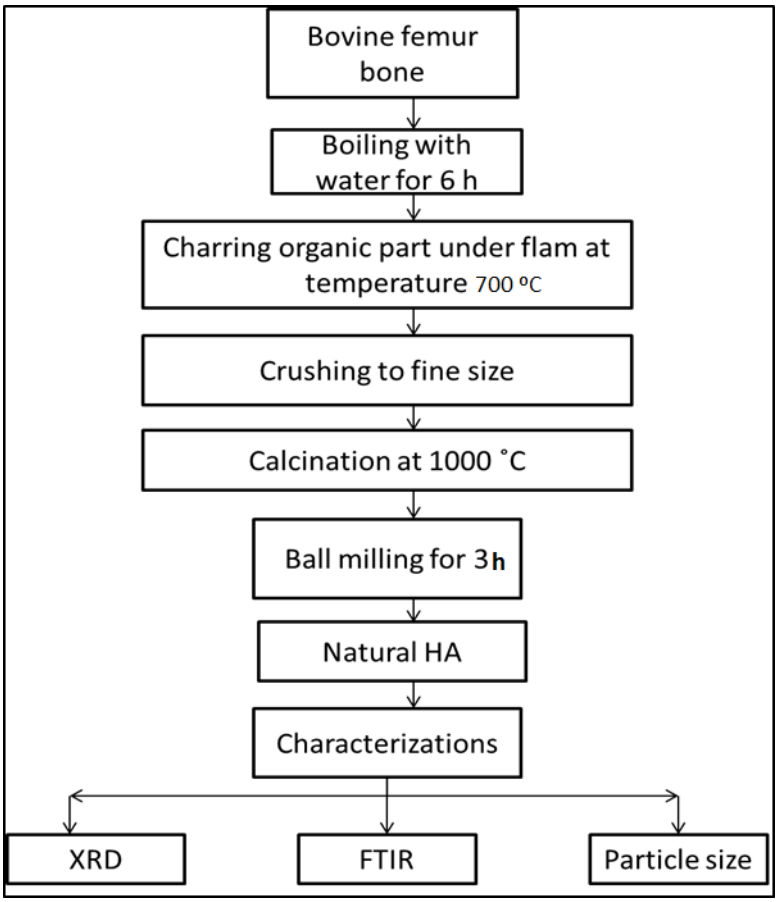

Figure (4.2) Flowchart depicting the process of extracting HA from bovine bone.

4.3 Preparation of HA and Composite Specimens

For studying DIC and the DIC procedure, the composites were made with HA powders obtained in the lab and commercial PSZ powder.

Mechanically mixing HA powder with PSZ nanoparticles (80 nm) in various quantities yielded the powdered mixture intended for sintering.

Four mixtures were obtained based on the PSZ concentration (HA/5, 10 ,15 and 20 wt % PSZ) in this step. They were mixed with ethanol for 6 hrs. The resulting slurry dried at 100 ˚C in an oven for 12 h. After that, The dry powder has already been crushed and sieved to produce powder to the compact.

4.3.1 Compact of HA and Composite

Poly vinyl alcohol (PVA) (2 % wt) was combined with HA powder and composite powders as a binder. The study uses a uniaxial semi-dry pressing technique. A rectangle mould constructed of stainless steel with dimensions of (60*6*5 mm) was utilized to manufacture the compacts. The required pressure was 150 MPa. Compacts were sintered under 1250°C for 3 h at a rate of heating 5°C/min, then cooled within the furnace.

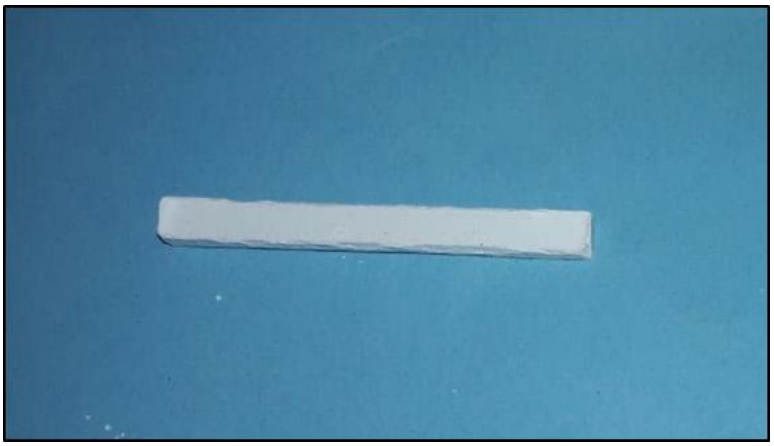

Figure (4.3) Sample after sintering.

4.4 Measurement of Porosity and Density

The density of sintered compacts was measured in accordance with ASTM C 20. The following of the steps within this method:

- The test samples were dried for 24 h at around 100˚C. The weight dry (D) was measured after cooling the desiccators at room temperature.

- The specimens were heated for 5 h in the distilled water in a beaker, with the Water covering the samples at all times. The specimens were left to soak for 24 hours after boiling. The suspended mass (S) of the tested specimens were measured after impregnation.
- The samples were lightly rolled on a moist cotton cloth to eliminate any extra water from its surface after (S) was determined, then weighed to determine the saturated mass (M)[95].

The bulk density (ρ) and apparent porosity (P) are defined as shown in the equations (4.1) and (4.2), respectively :

$$Bulk\ density = D/(M - S) \quad \text{.....(4.1)}$$

$$Porosity\ \% = \frac{M-D}{M-S} \quad \text{.....(4.2)}$$

4.5 Grinding and Polishing

The specimens were ground with a rotational speed of 300 rpm on (YMP – 2 Device, Department of ceramics and building materials - college of materials Engineering -University of Babylon)with Grinding papers made of SiC in various grit sizes (140, 180, 320,600, 800, 1000, 1200, 1500, 2000). The grinding time (10 min) for each one, Water is frequently utilised as a cooling agent.

After grinding, the polishing process was carried out on the same machine, but with a polishing cloth instead of SiC paper. The polished specimen is shown in Figure (4.4)and (4.5).

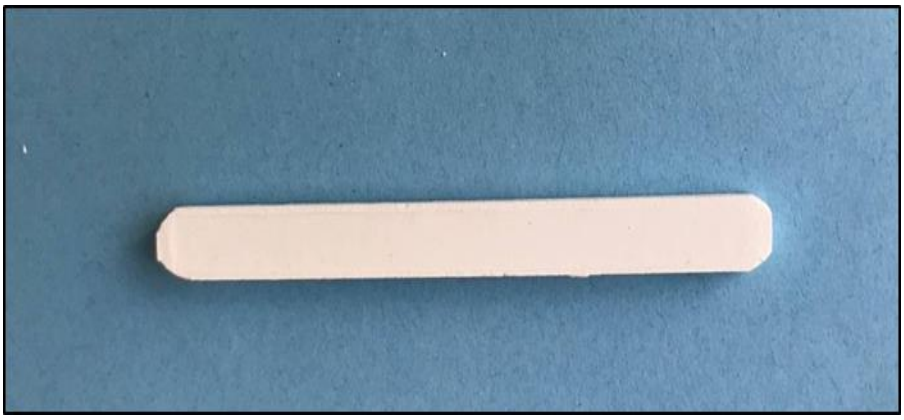

Figure (4.4) Sample after grinding and polishing.

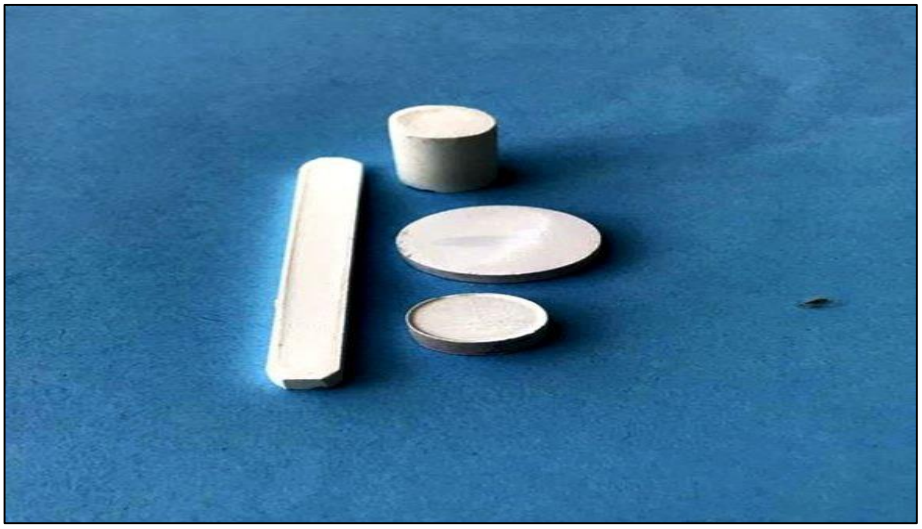

Figure (4.5) Samples for physical and mechanical tests

4.6 Characterizations

4.6.1X-Ray Diffraction (XRD)

X-ray diffraction is a procedure that employs X-rays to analysis phase composition and assess structural features of powders and composites. This approach produces the same diffraction pattern for each phase in a substance, regardless of whether it is pure or a mixed X-ray diffractometer. (XRD 6000, Shimadzo, Japan, Department of ceramics and building materials - college of materials Engineering -University of Babylon), used at ambient temperature (Cu kα) radiation λ = 1.5405Å,

5º/min as the speed of scanning from 10◦ to 65◦ of 2θ (angle of Bragg) and 40 kv/30 mA is the power that is used**.**

4.6.2 Fourier Transform Infrared Spectrometer

Infrared spectra (FTIR) of the sample were recorded using (Shimadzu1800,Japan) to analyse the molecular structure of the functional group for inorganic material. Tests were done in (Department of Polymer Engineering and Petrochemicals Industries - college of materials Engineering -University of Babylon).

4.6.3 Scanning Electron Microscope (SEM)

The crack propagation of HA and HA/ZrO_2 composite specimen and the homogeneity of the composite material were investigated by using a scanning electron microscope and energy dispersive X-ray. (SEM – Germany, 2013 at the Material Engineering Department, College of Engineering, University of Tehran) was used to test the specimens. The study uses a plasma-sputtering process, and the samples were first coated with Au.

4.6.4 Particle Size Analysis (PSA)

A Bettersize2000 laser particle size analyser was utilized to assess the particle size distribution of HA particle , which is positioned (Department of ceramics and building materials - college of materials Engineering -University of Babylon) (Better size instrument Ltd., China).

4.7 Calculation of Mechanical Properties

Three specimens were tested at the same conditions for each test to determine the average value.

4.7.1 Compression Strength

The compression strength of the material was measured via a universal electrical testing machine (WDW-5E , Department of Polymer Engineering and Petrochemicals Industries - college of materials Engineering -University of Babylon). with a test speed of 0.5 mm/min. Dimensions of cylinder specimens (D=10mm, H=20mm).

The compression strength was estimated using the following formula, which was completed in accordance with ASTM C-1424[96]:

$$\sigma c = \frac{Pf}{A_o} \quad \text{.....(4.3)}$$

Where :

σc= Compression strength MPa

Pf = Load of fracture N

A_o = cylinder specimen cross section area mm^2.

4.7.2 Vickers Hardness

Steel dies were used to prepare disc specimens (diameter=13mm, height=5mm), and all specimens were correctly polished. A digital micro Vickers was used to do the test.

In accordance with ASTM standard C1327-90, a hardness tester TH-717 was applied 1kg with keep dwelling for 15 sec. The following equation was used to determine Vickers hardness:

$$Hv = 1.854(\frac{p}{d^2}) \quad \text{.....(4.4)}$$

Where:

Hv= Vickers hardness MPa

p =load N

d = the indentation impression's diagonal length mm.

4.7.3 Bending Strength

This test was done using the rectangular bar specimens prepared with dimensions (50*4*3 mm). This test was carried out utilising an ASTM C1161 computerised universal testing equipment with a 0.5 mm/min test speed. To calculate the bending strength, the following equation was utilised.

$$\sigma b = 3pf\ L/2wt^2 \ldots\ldots\ldots (4.5)$$

Where:

σb = bending strength MPa

pf = the load of fracture N

L = length of span mm

w = sample width mm

t = thickness of sample mm [97]

4.7.4 Fracture Toughness (KIC)

Fracture toughness of HA and composite specimens was measured with single edge notched beam method , according to ASTM C1421 and the equation (4.6) [98].

$$K_{Ic} = g\left[\frac{P_{max}\ S_o\ 10^{-6}}{BW^{3/2}}\right]\left[\frac{3[a/W]^{1/2}}{2[1-a/W]^{3/2}}\right] \ldots\ldots\ldots (4.6)$$

This equation for three-point flexure with $5 \geq S/w \leq 10$ and a/w = 0.2 - 0.3.

Where:-

KIC is fracture toughness MPa .√m, Pmax is maximum load N ,So is span between support ,B is width of sample ,W is specimen height ,a is crack length and g is coefficients , for g depends on the ratio of (S/W).

$$g = g\left[\frac{a}{w}\right] = A_o + A1\left(\frac{a}{w}\right) + A2\left(\frac{a}{w}\right)^2 + A3\left(\frac{a}{w}\right)^3 + A4\left(\frac{a}{w}\right)^4 + A5(\frac{a}{w})^5$$

The value of (Ao, A1, A2, A3, A4 and A5) were determined from tables in ASTM 1421. In the experimental work, the S/w ratio was 10, a/w was 0.22 – 0.26, and the notch width was ~120μm.

4.7.5 Single Edge Notch Beam Method

A single edge notch beam was used to prepare the specimens for fracture study. Figure (4.6) depicts a sketch of a specimen with dimensions of 50*4*3 mm. A 100 μm thick diamond-coated dental disk was used to create the notch, as indicated in figure (4.7).

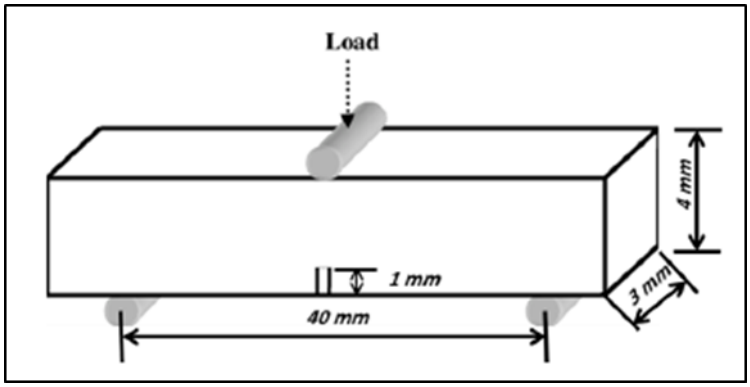

Figure (4.6) Sketch of specimen.

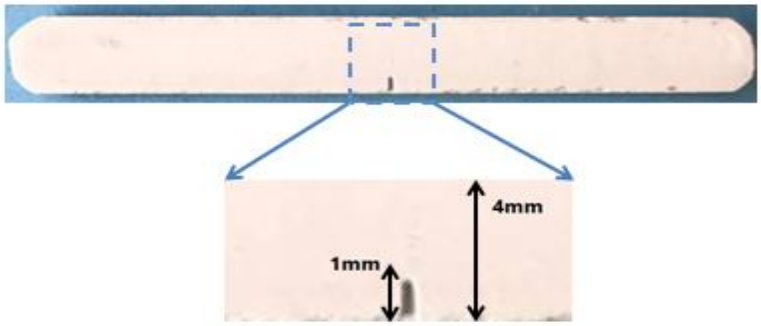

Figure (4.7) Notched specimen**.**

4.8 Digital Image Correlation Test

The Digital Image Correlation (DIC) technique is an optical technology that measures deformations and displacements in full-field, non-contact, and high precision. A uniform coat of white paint was added to the surface to create a uniform background. Spraying a black mist on the specimen surface produced the sprayed-on speckle, which was created by painting (vinyl cetate/ethylene VAE) on the specimen surface, as shown in figure (4.8)

Figure (4.8) Specimen surface with black paint

The speckle pattern must be non-repetitive, isotropic, and contrast enough for the program to differentiate between the image before and after deformation. To make a subset, the specimen must be sprayed

GOM (Gesellschaft fur Optische Mebtechnik), a German corporation, provided the DIC calculation program. This approach starts with a pre-loading reference image, which is then compared to a sequence of pictures

obtained during the loading process. According to one hypothesis, the colour value of the photographs is assumed to be the same before and after deformation. The photos were first divided into several subsets. Then a deformation or displacement distribution map was constructed by searching for the corresponding subsets following deformation based on the assumptions and calculating their displacements. The Subset on the Surface is depicted in Figure (4.9).

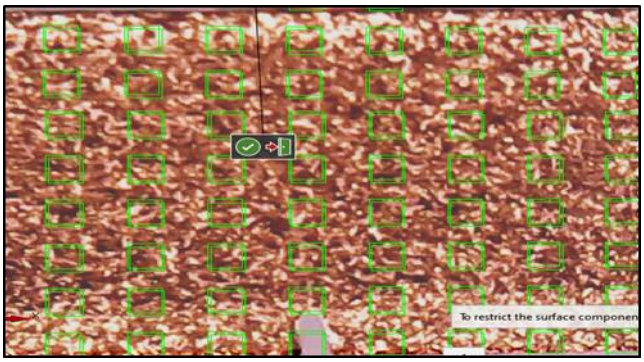

Figure (4.9) Subset show when Speckles of black paint.

The flowcharts for preparing the sample for studying crack propagation and crack opening displacement can be displayed in Figure (4.10).

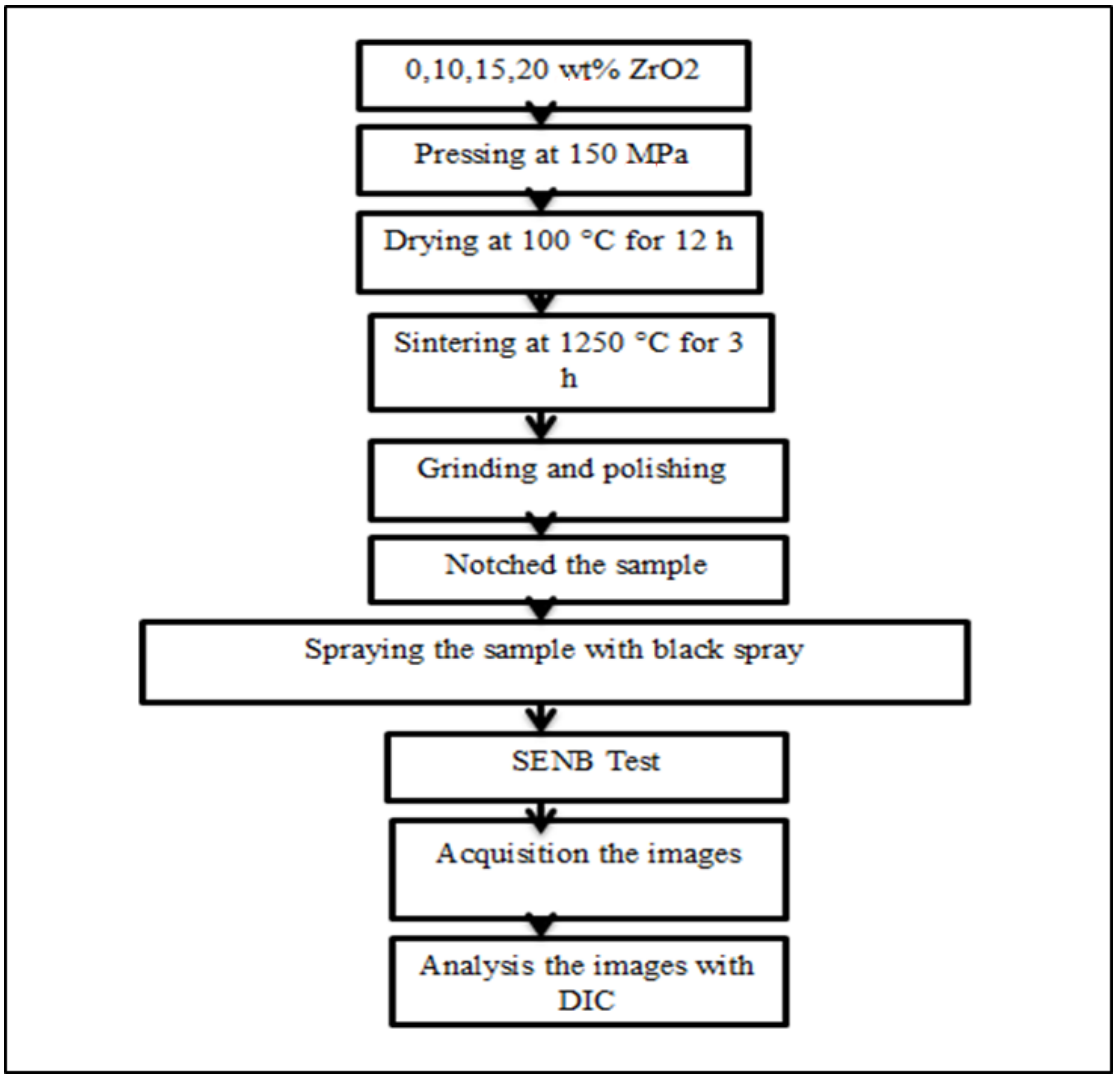

Figure (4.10) Flow chart display of DIC procedure.

4.8.1 Loading Setup and Test Procedure

Specimens were subjected to the load microcomputer controlled electronic universal testing unit, as shown in figure (4.11). The loading capacity of this testing machine is (5 kN), the loading rate is low, resulting in a displacement of less than (0.005 mm/min). A digital microscope camera (Genesys Logic) with the following features:

A lamp was employed to brighten the speckle pattern and take digital photos during the loading process. The camera was set up so that the lens was as parallel to the specimen surface as possible, and the focal length was adjusted to give a clear image. The resolution of the camera was set to

640 480 pixels, then the imaging system's length-pixel ratio was set to 0.0008 mm/pixel. The camera was designed to capture images at a frame rate of 10 (10 pic/sec) automatically, which is ideal for the capturing and storing a big number of photos to be used in later calculations.

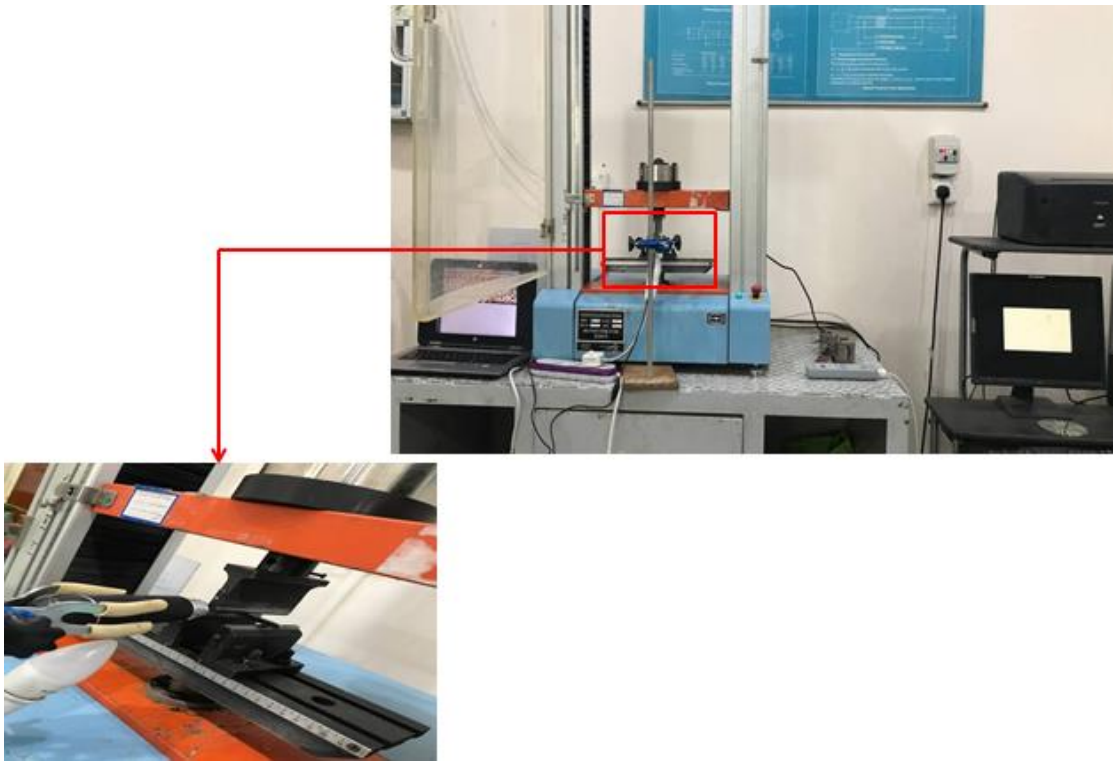

Figure (4.11) Setups loading.

4.8.2 Crack propagation and opening using DIC

Crack propagation and opening were studied by using DIC (GOM). After running the program, the images were imported into GOM software to analysis all images to observe the cracking.

4.8.2.1Measurement of the crack opening displacement

Figure (4.12) shows the crack mouth location and crack tip opening displacement. The two curves method can be used to estimate the crack opening displacement (CMOD and CTOD) by DIC, as shown in figure (4.13). By analyzing how the distance between two curves deviates from a reference value, the crack opening computation with distance checks can

be performed. In the first active step, the reference value can be a nominal or a distance.

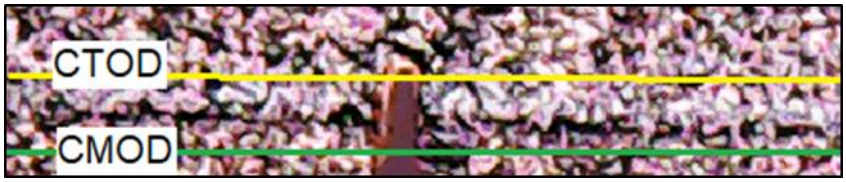

Figure (4.12) The Position of CMOD and CTOD in GOM.

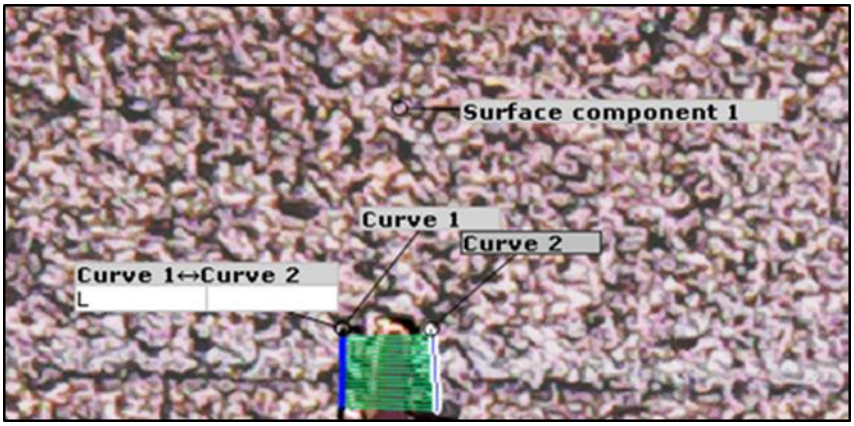

Figure (4.13) Measurement of CMOD and CTOD by curve method.

Chapter Five

Results & Discussion

5.1Introduction

This chapter explains the results gained by the experimental work, and in addition, it gives a clear discussion about these results. The first section in this chapter is related to experimental work and the second section displays the outcome of the GA technique**.**

5.2 Characterization of Powder

5.2.1 X-Ray Diffraction

XRD examination of bovine bone after it was calcined at 1000°C for three hours display in Figure(5.1) , The XRD analysis of HA after sintering for three hours at 1250°C is shown in Figure (5.2) that explain the peaks are more sharp and crystalline than when sintered at 1000°C . All peaks agreement with (JCPDS, card NO. 01-074-0866).

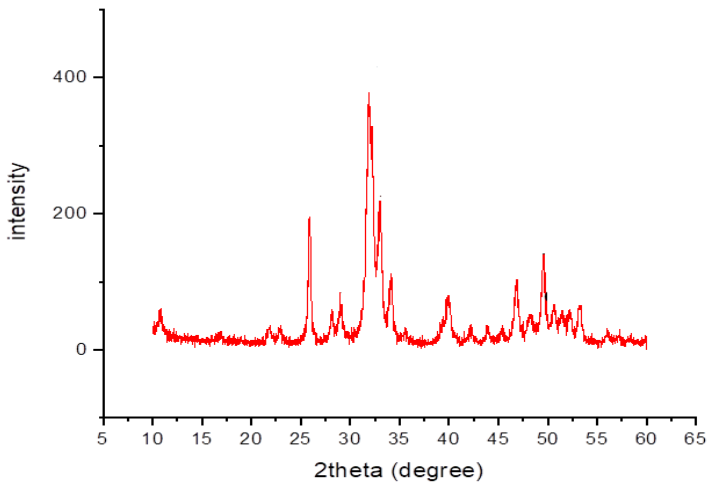

Figure (5.1) The XRD of raw bovine bone after it has been calcined.

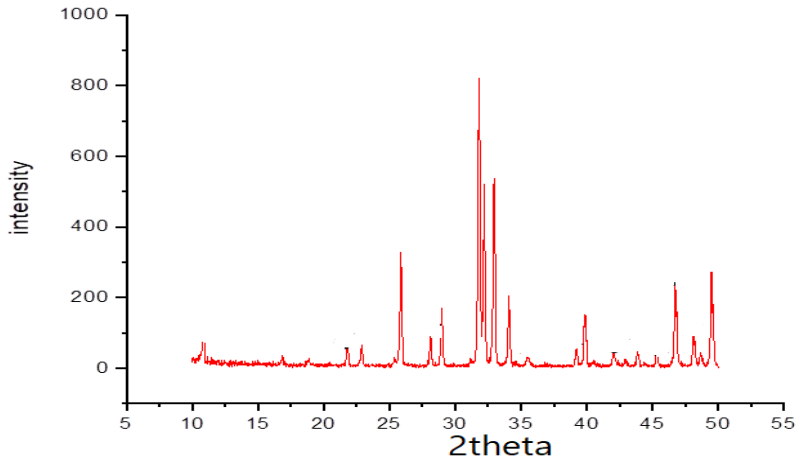

Figure(5.2) XRD of hydroxyapatite after sintering at 1250˚C.

5.2.2 Particle Size Analysis.

Figure (5.3) shows the particle size (P.S) distribution analysis of the results for hydroxyapatite powder after milling for 3 h. The hydroxyapatite particles were distributed in a range of 0.3 to 3 μm. (0.30, 0.84, and 3.77, respectively) for D10, D50, and D90.

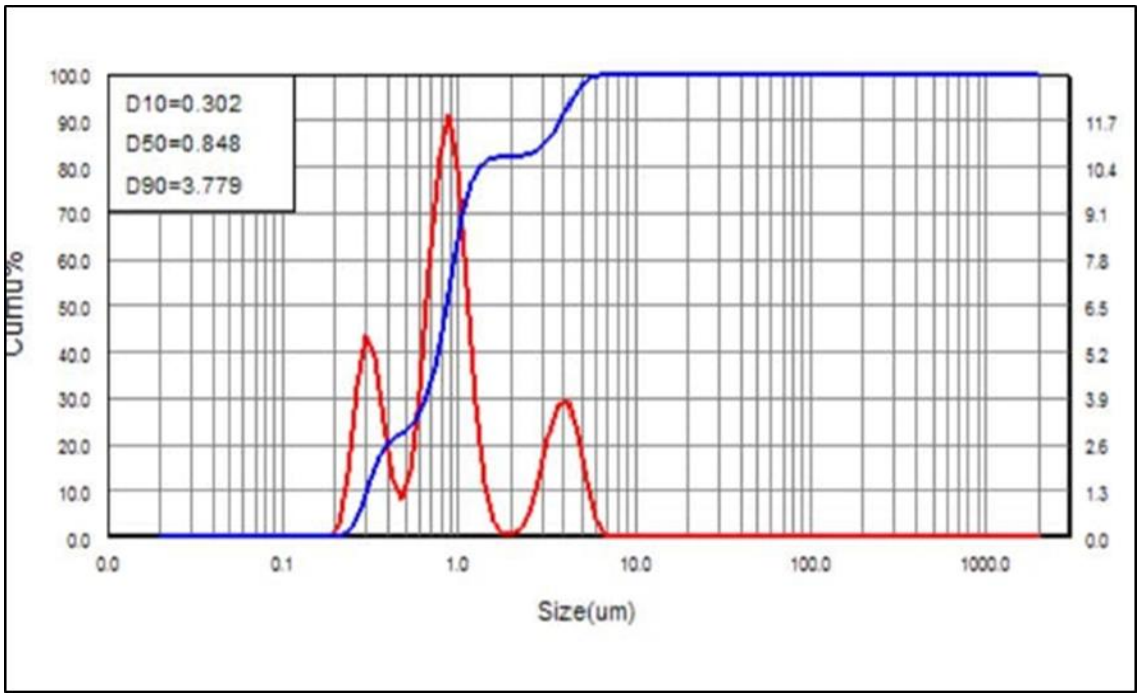

Figure (5.3) The Analysis of particle size distribution of HA powder

5.2.3TheFourier transforms Infrared Spectrometer.

The specimen was characterized infrared to investigate the spectrum characteristic denotes the presence of chemical bonds in the produced HA. The peak around 3417.86 cm-¹ in Figure 5.4 is due to the presence of an O-H bond. The O-H stretching vibration in HA is mostly responsible for this peak. The mechanisms of stretching of HA's P-O bonds are connected with the peak at 1033.85 cm-¹. The bending modes of P-O bonds in phosphate groups are responsible for the double peak at 601.79 cm-¹ and 570.93cm-¹. The reference was used to determine the FTIR result of HA powder [99].

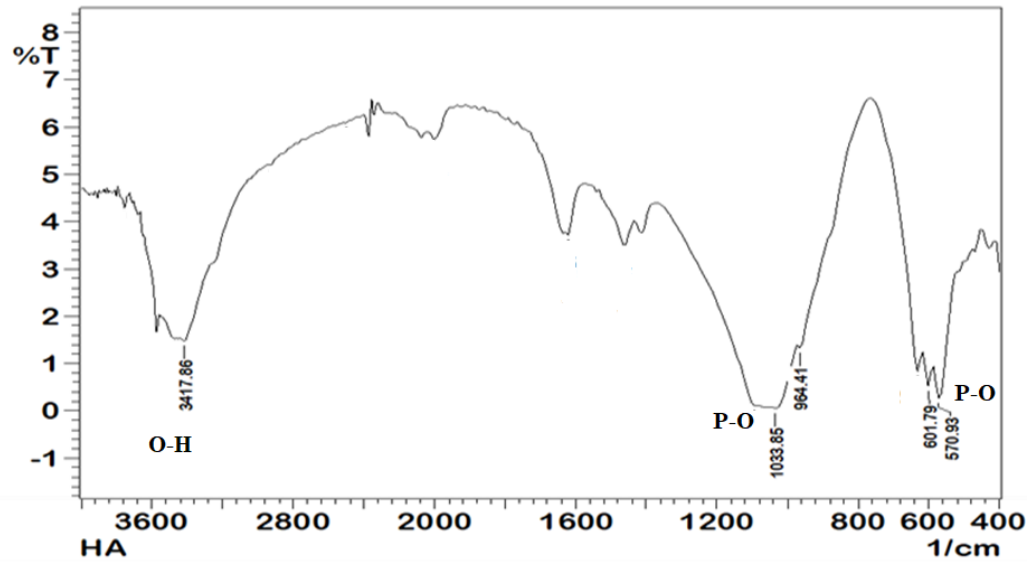

Figure (5.4) The FTIR of HA powder.

5.3Characterization of synthesized Samples

5.3.1 X-Ray Diffraction.

Zirconia's powder XRD which its peaks agree with all peaks of (JCPDS, card No.00-049-1746) shown in figure (5.5). Figures (5.6) ,(5.7),(5.8),(5.9) display XRD for HA/5,10,5,20PSZ% , respectively. These samples were heated at 1250 C for 3 h with 5 C/min . XRD analysis is done from 5˚ to 55˚ to appear the essential peaks in the cards.

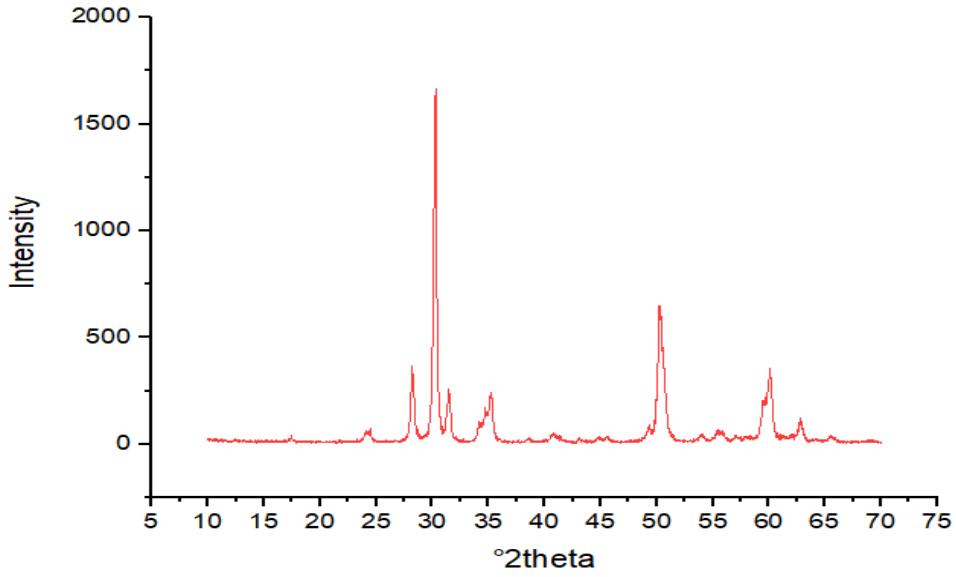

Figure (5.5) XRD for PSZ powder.

Figure(5.6) shows that hydroxyapatite was found as the main phase with the presence of peaks for PSZ and a small percentage of βTCP (Whitlockite) which increased with increase of PSZ (Baddeleyite) .Where the figure(5.9) shows at the ratio of PSZ used 20% that the hydroxyapatite phase it may decompose a large extent to βTCP . All peaks of βTCP agreed with (JCPDS, card No.00-009-0169) and peaks of PSZ agreed with (JCPDS, card No.00-037-1484) .

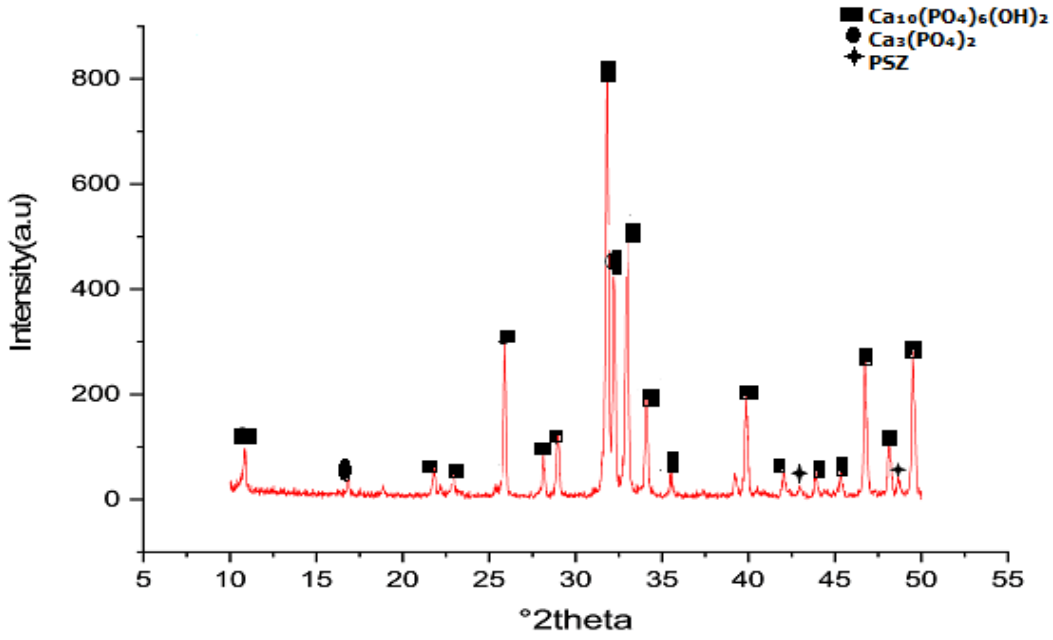

Figure (5.6) XRD of HA/5PSZ% composite .

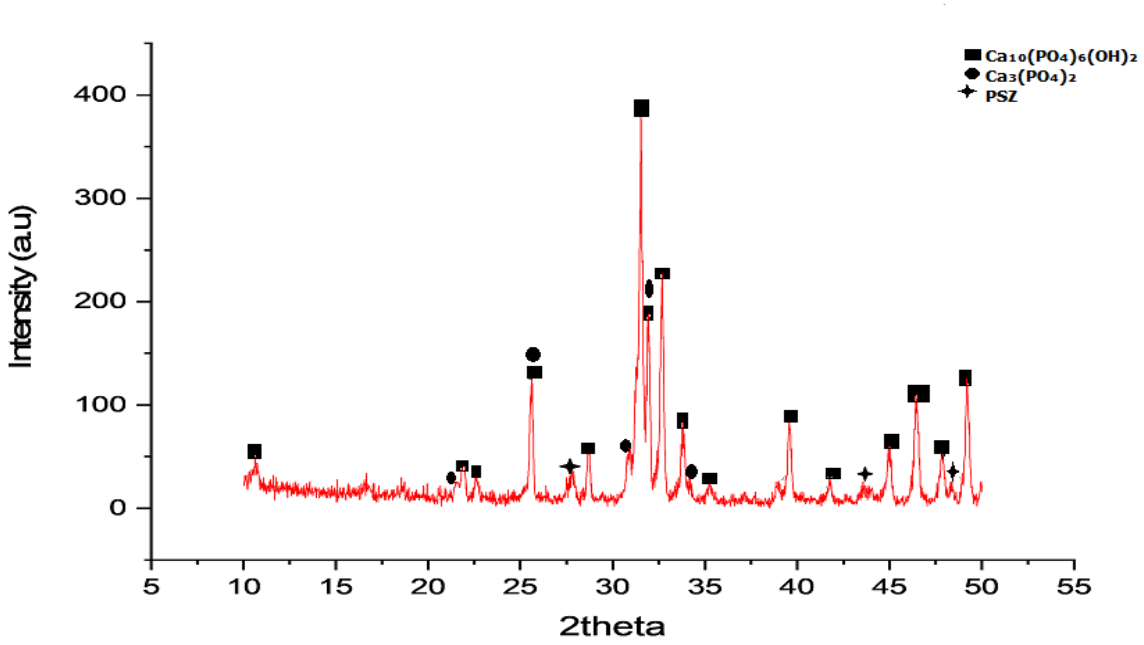

Figure (5.7) XRD of HA/10PSZ% composite .

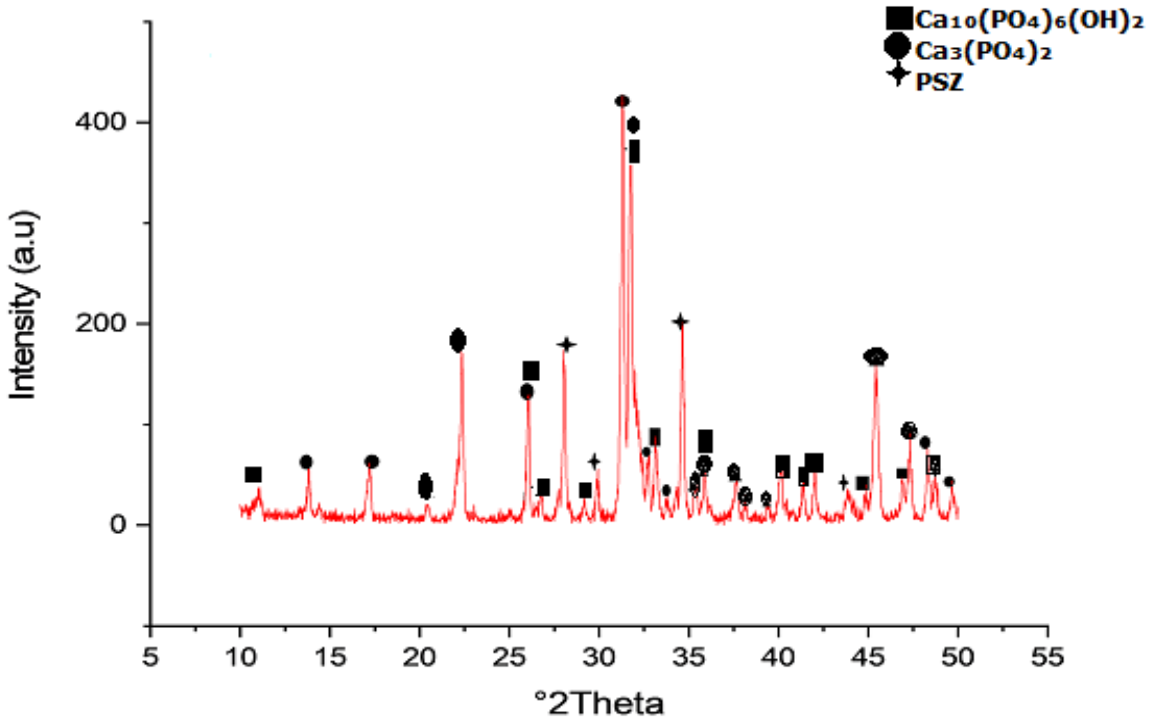

Figure (5.8) XRD of HA/15PSZ% composite .

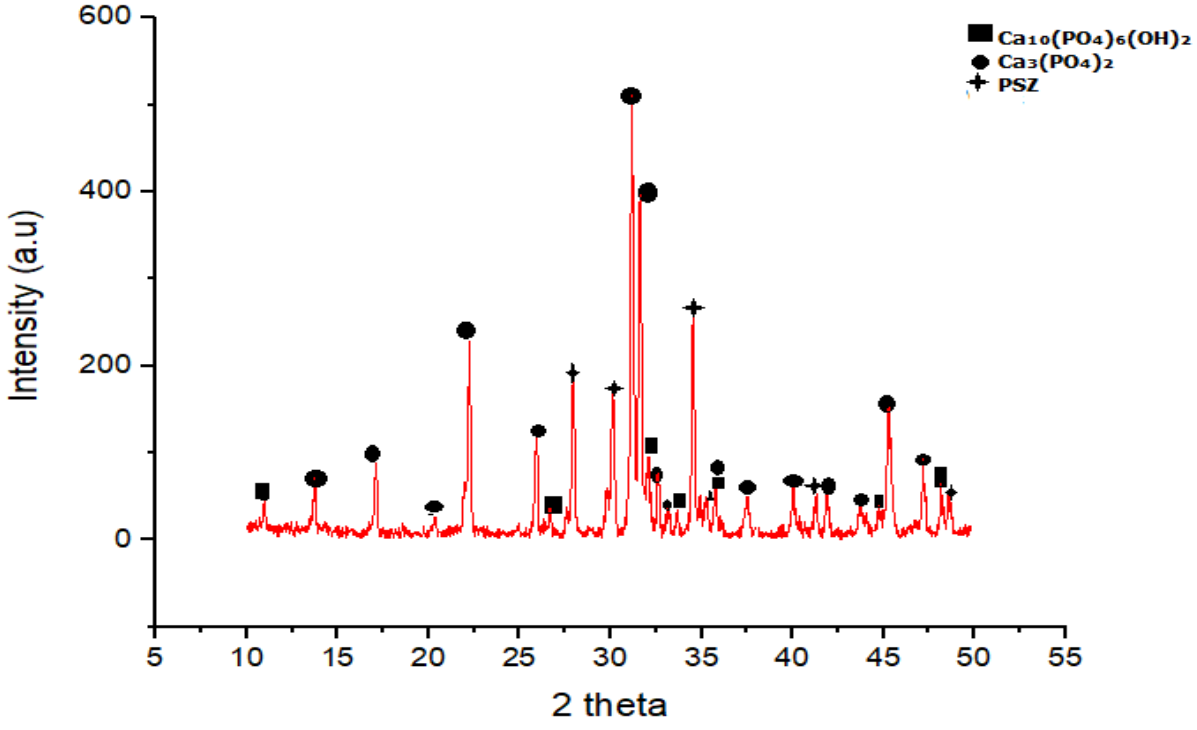

Figure (5.9) XRD of HA/20PSZ% composite .

5.3.2 The physical properties

The bulk density is considered one factor that affects ceramic materials' mechanical and physical properties. Figure (5.10) represent the effect of PSZ content on the density of the compact samples. The high value of The density at (HA /5 wt .% PSZ) is (3 g/cm³) and then begins to decrease with the increase in the amount of PSZ gradually.

Figure (5.11) shows the apparent porosity of the compact samples, where the study noticed that the porosity began to decrease, where it was the lowest porosity obtained at (HA /5 wt .% PSZ) is (13 %) and then began to increase with the increase in the amount of PSZ gradually.

The main reason for the increase in porosity with the increase in the amount of PSZ despite its high density, which reaches approximately 6 g/cm³ is the high melting point of zirconia, which needs sintering at high temperatures, for this reason the densification decreases .

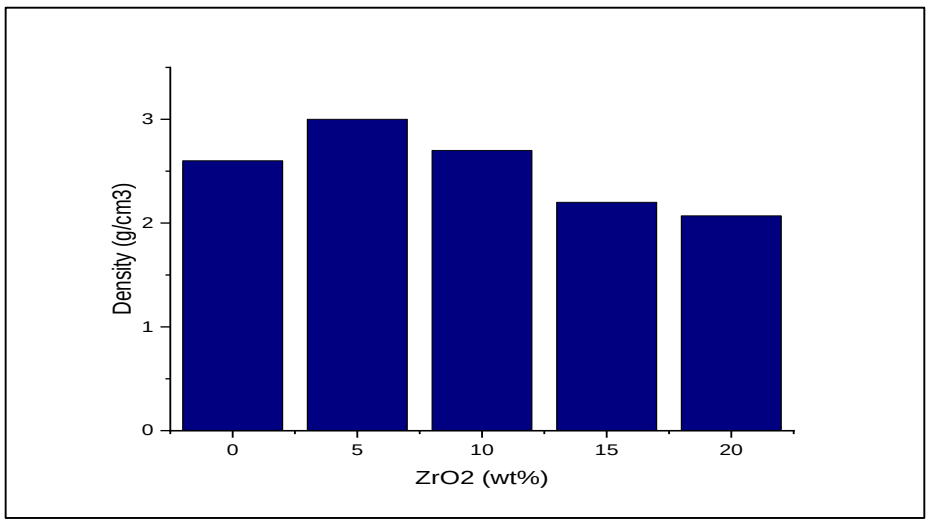

Figure (5.10) The effect of PSZ on density.

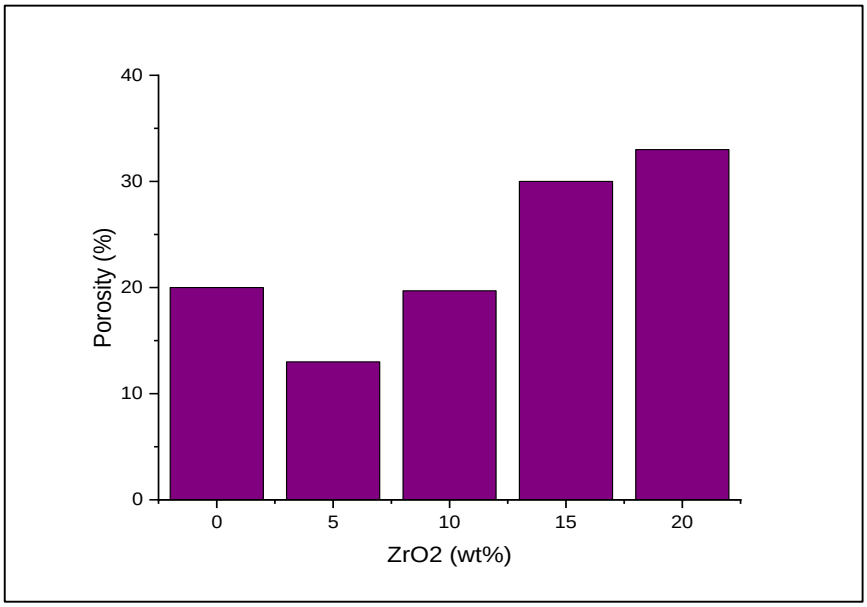

Figure (5.11) The effect of PSZ% on porosity.

5.3.3The Mechanical Properties

Figures (5.12),(5.13),(5.14) and (5.15) shows the results of the composite's mechanical properties. The highest values of the composite's mechanical properties were obtained at (HA/5PSZ wt%). Where the hardness is (3.8GPa), compression is (98 MPa), bending is (43 MPa), and fracture toughness is (1.1MPa.√m). Then begin to decrease with the increase in the amount of PSZ gradually.These results agree with the physical results obtained, where the reason for the improvement of the properties in HA/5wt%PSZ is due to the improvement of the density in this ratio. In other words, The increase in densification and thus a decrease in porosity due to the temperature used. Perhaps due to the volume change accompanying the phase transformation process between the monoclinic and tetragonal phases.[71]

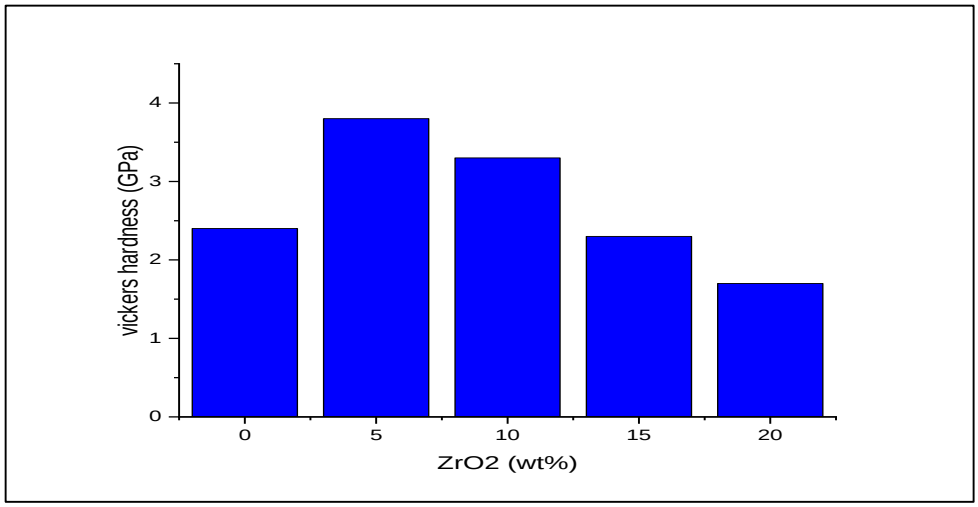

Figure (5.12) Effect of PSZ% on the Vickers hardness.

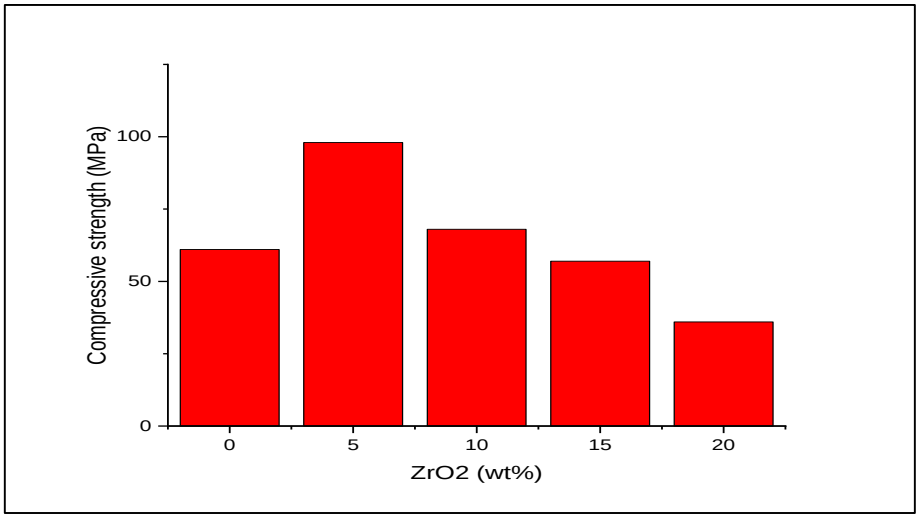

Figure (5.13) Effect of PSZ% on the compressive strength.

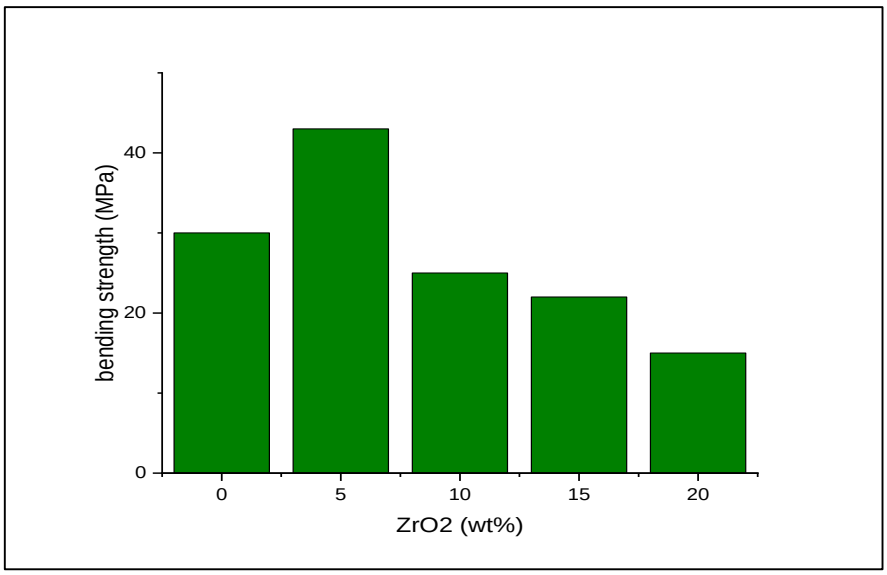

Figure (5.14) Effect of PSZ% on the bending strength**.**

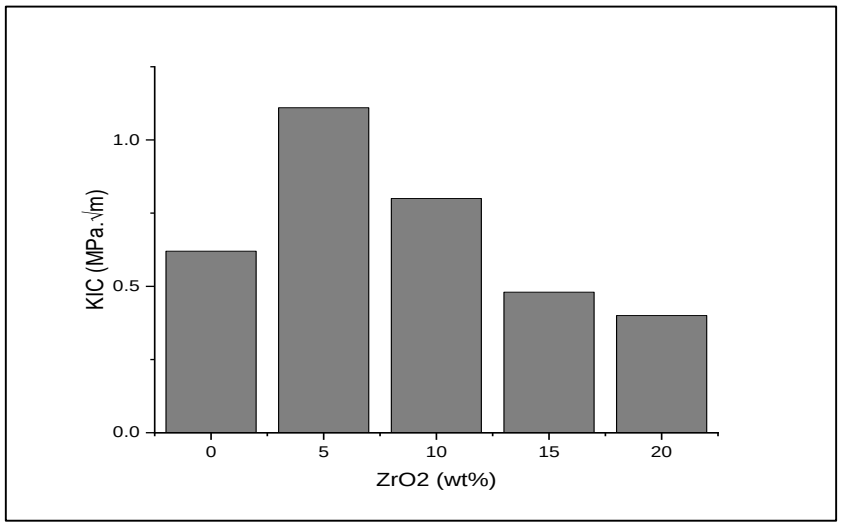

Figure (5.15) Effect of PSZ% on the KIC.

Vickers' indentations were studied into the toughening processes that occurred on polished surfaces, and the crack propagation path was as seen in Figure (5.16). Transformation mechanism toughening happens when the metastable phase (t-ZrO_2) retained in the tensile stress field surrounding a propagating of fracture converts to the stable phase (m-ZrO_2). The t - m martensitic transformation's volume expansion (4–5%) provides net compressive stress surrounding a crack tip in the process zone. This lowers the local crack tip stress intensity and, As a result, is the crack propagation's driving force, Increasing the effective toughness of ceramics [100].

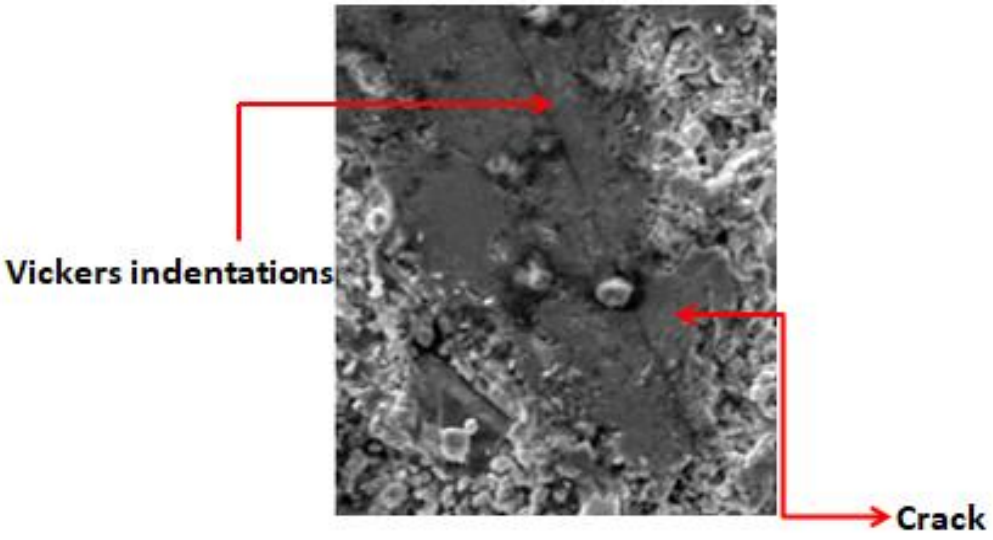

Figure (5.16). SEM for HA/5PSZ% sample

5.4 Digital Image Correlation

5.4.1Crack Propagation of Samples

Figures (5.17,18, and 19) illustrate the results of DIC to determine crack propagation with load and time in pure HA and composites, respectively. The change in strain mapping around the notch under various load and time for HA and composites specimens is shown in these figures. There are six pictures in each Figure. In all Figures, picture (a) depicts an undeformed specimen (before loading), image (b) does not depict a change in strain mapping near the notch tip, but image (c) depicts a change in strain mapping near the notch tip, indicating a stress concentration at the notch tip. As indicated in the illustration, a critical load and fracture have occurred (d). As illustrated in photos (e) and (f), the specimen loses its bearing capacity after that, and the load rapidly decreases as the break propagates (f).

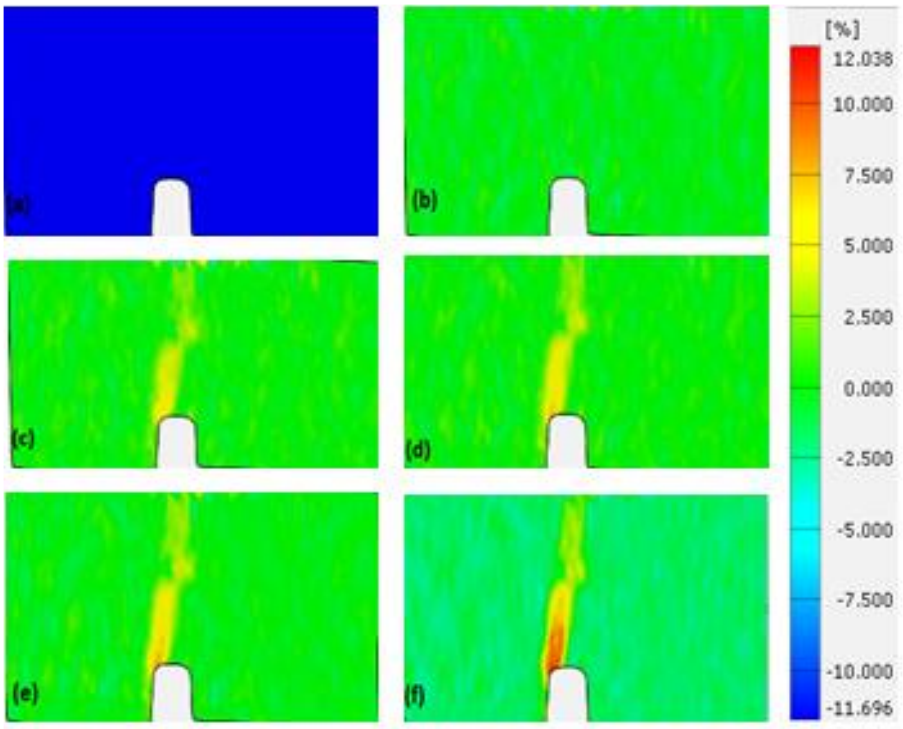

Figure (5.17) Strain maps of (HA) with different load and time. (a) P=0 N, t=0 s, (b) P=3N, t=76 s,(c) P=7N, t=270 s,(d) P=9 N, t=308 s,(e) P=6 N, t=322 s, (f) P=4N, t=344 s

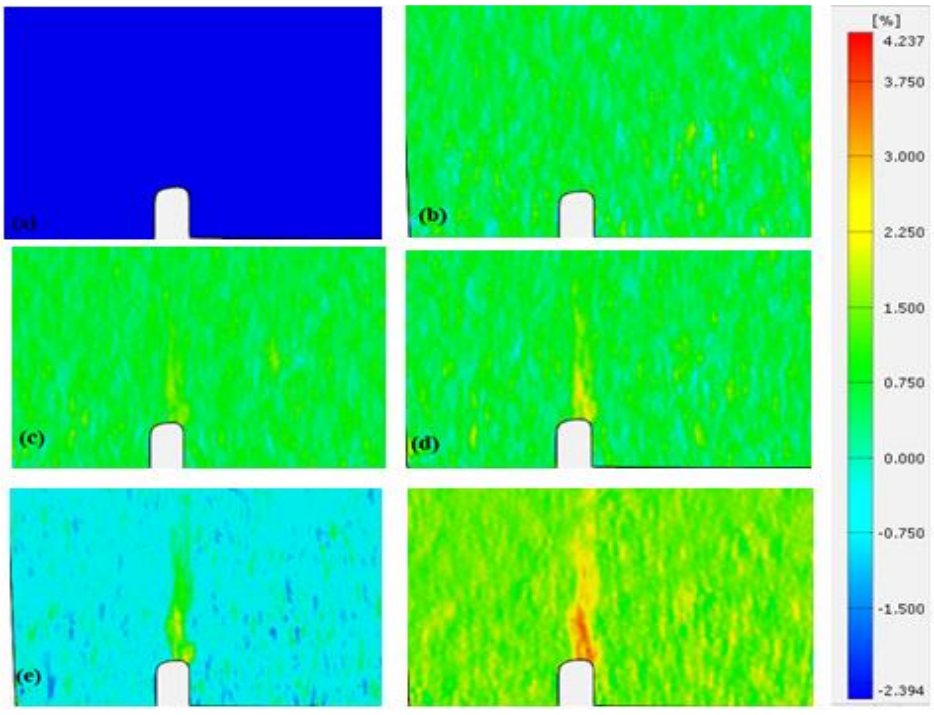

Figure (5.18) Strain maps of (HA /5PSZ %) with different load and time. (a) P=0 N, t=0 s, (b) P=8N, t=561 s,(c) P=12N, t=683 s,(d) P=17 N, t=862 s,(e) P=15 N, t=875 s, (f) P=9N, t=877 ***s***

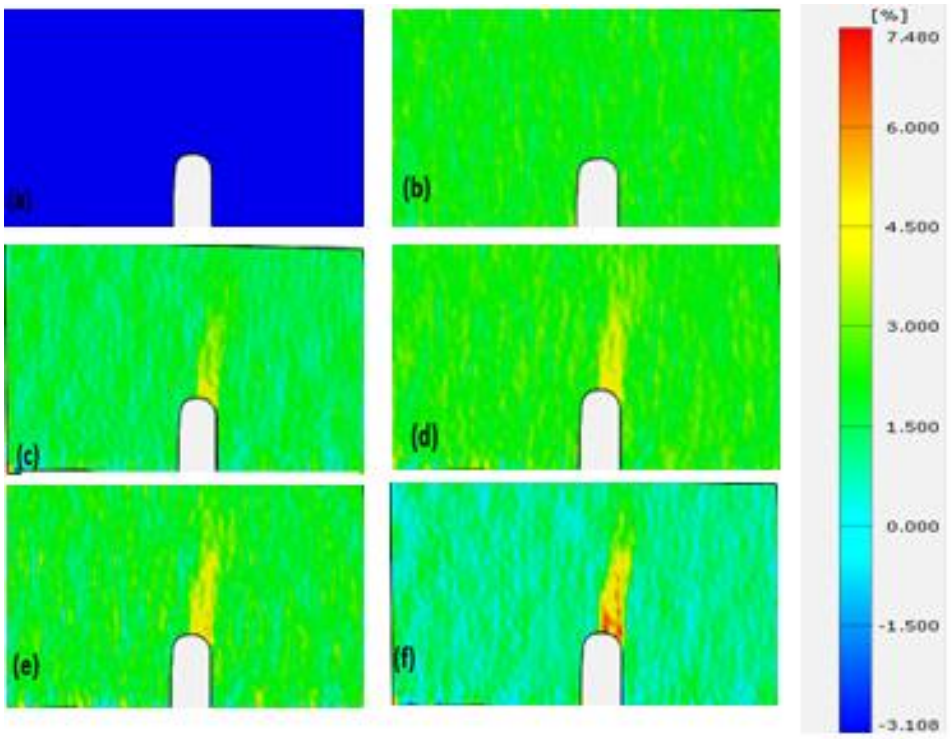

Figure (5.19) Strain maps of (HA /10PSZ%) with different load and time. (a) P=0 N, t=0 s, (b) P=4N, t=300 s,(c) P=8N, t=460 s,(d) P=12N, t= 580s,(e) P=8N, t=583 s, (f) P=4N, t=585

In the SENB approach, the relationship between Load and time is shown in Figure (5.20). The crack initiation time was 308 secs and the critical load for HA (9 N). In addition, the critical load for (HA /5 PSZ %)is (17 N) at a critical duration of 862 sec, as shown in Figure (5.17). At critical time 580 secs, the critical load for (HA /10PSZ %) (12 N) The addition of less than 10% PSZ to HA improved its fracture toughness.

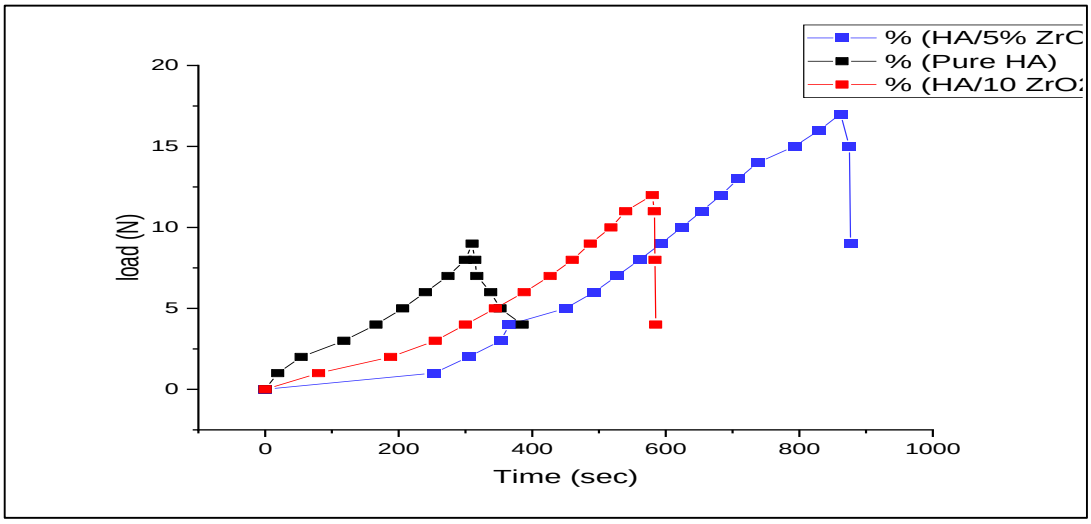

Figure (5.20) The relation between Load and time

5.4.2Crack opening of specimen

Figures (5.21) and (5.22) shows the relationship between applied force and crack opening displacement (CMOD and CTOD). The force against CMOD curve for pure HA can be separated into three parts, as seen in this diagram. The relationship was linear in the first part. The second part began As soon as the curve began to diverge from linearity. The opening of the crack begins to accelerate, suggesting the onset of material deterioration. In this part, the Load continued to increase until the peak load reached a critical value, and the material could not go beyond this maximum loading capacity. After the peak critical load stage, the last part started when CMOD continued to increase, and the Load began to decrease. For curve, CTOD is split into two parts. The relationship is linear in the first part, and a linearity continues until it reach the peak load. After reaching the peak load, the crack opening increased as the applied Load was reduced. The specimen's crack opening displacement increased until it failed and the results of CTOD and CMOD for the composites it can be noticed that the two curve shapes (CMOD, CTOD) a little different from pure HA curved. It also divided into two parts. The relationship In the first part was linear until reaching a peak load (maximum Load).In the second

part, the tail of the curve shown the (CMOD, CTOD) increasing , while the Load decreasing gradually. The reason for the difference between the behaviour of the curves is due to the mechanism of toughening caused by PSZ addition, which delays crack propagation, later more energy is required to make the crack propagate.

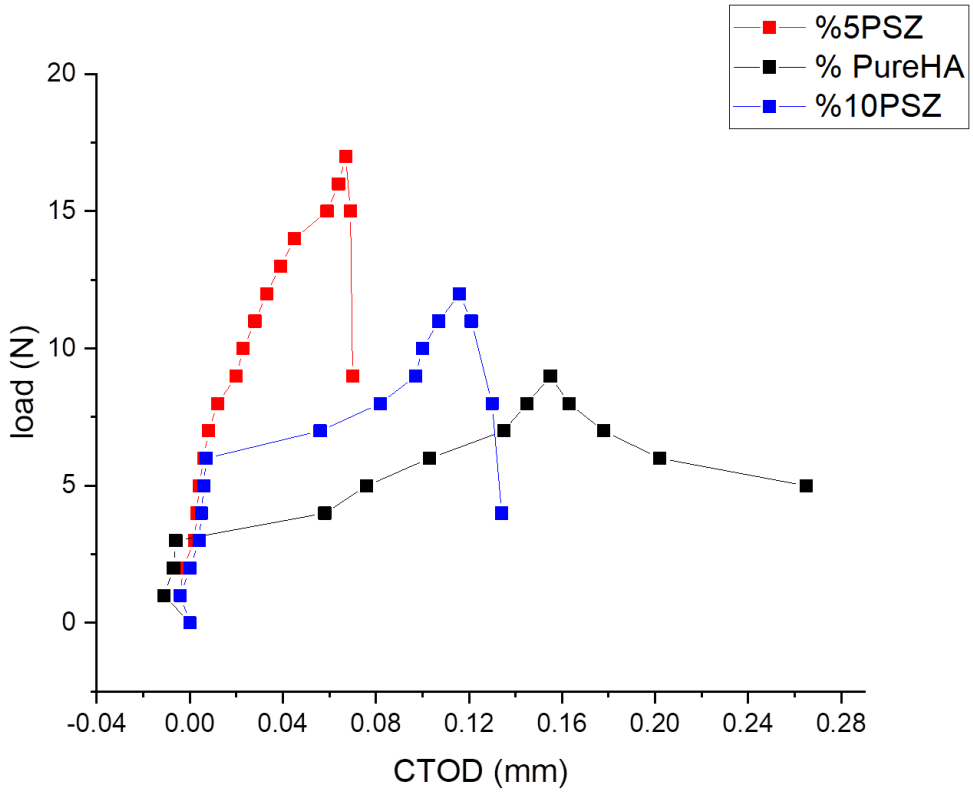

Figure (5.21) load versus CTOD for pure HA , HA/5%PSZ and HA/10%PSZ .

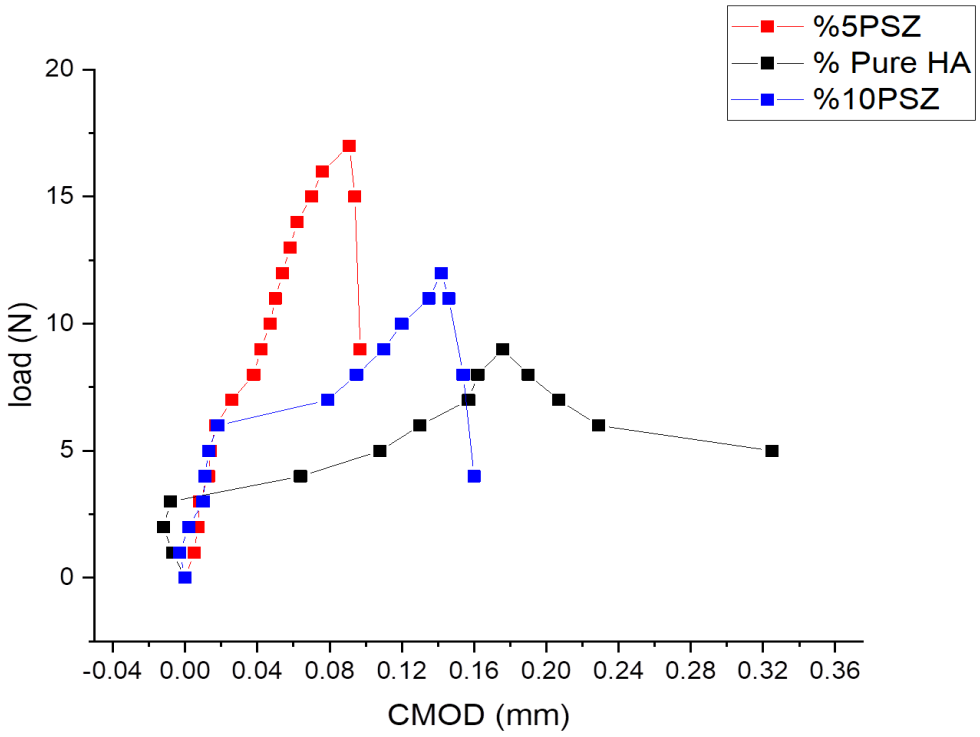

Figure(5.22) Load versus CMOD for pure HA ,HA/5%PSZ and HA/10%PSZ.

The relationship between COD (CMOD and CTOD) with the time of pure HA and composites is shown in Figures (5.23) and (5.24). For pure HA, it can be noticed that the rate of crack opening increased gradually until it reached the critical time. As well as, the rate of crack opening increased compared with before critical time. As for the composite have similar behaviour to pure but increase in time before reaching to critical Load.

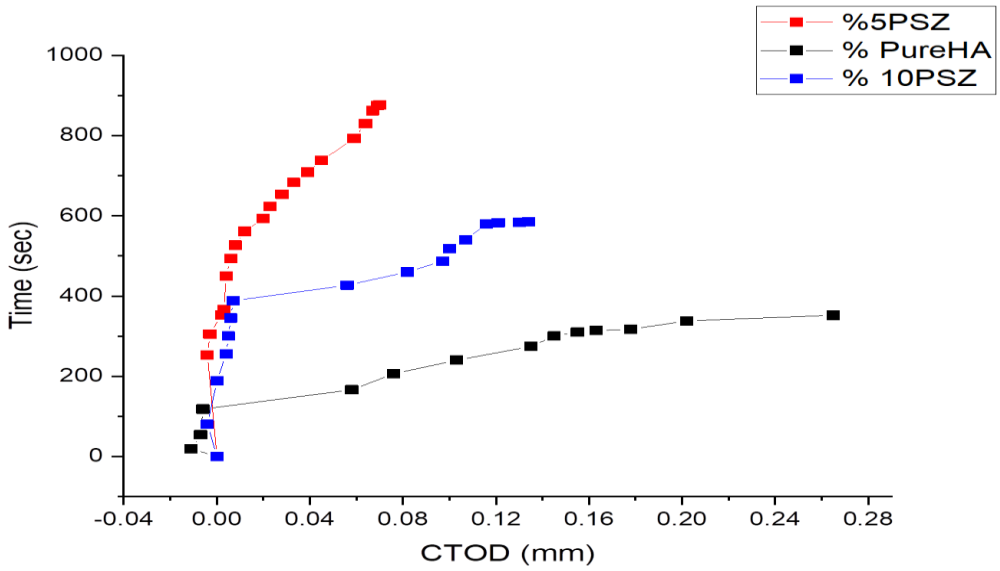

Figure (5.23) Time versus CTOD for pure HA ,HA/5%PSZ and HA/10%PSZ .

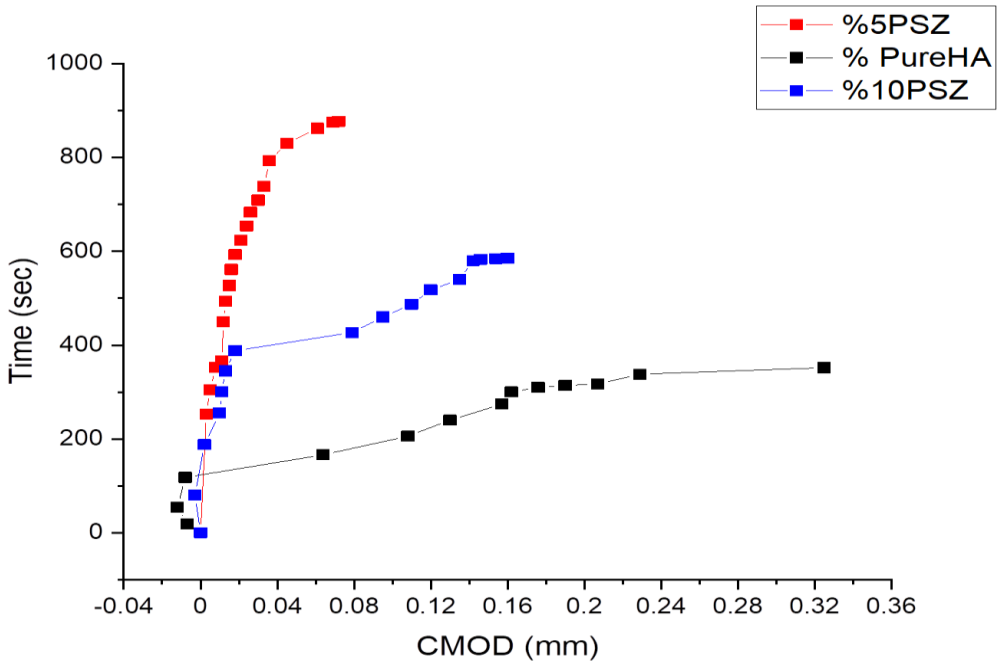

Figure (5.24) Time versus CMOD for pure HA ,HA/5%PSZ and HA/10%PSZ

The relationship between crack extension and Load is shown in figure (5.25). From this Figure, it can be noticed that the crack initiation of pure HA was at load 9 with a length of 0.55mm and continued propagation with force less than 9 N. In addition, this Figure shows that the crack initiations

were with length 0.28 mm at load 17 N for (HA/5PSZ%) and (HA/10 5PSZ%) the crack initiated with load 12 N with length 0.435mm and both specimens are continued propagation with force less than critical Load.

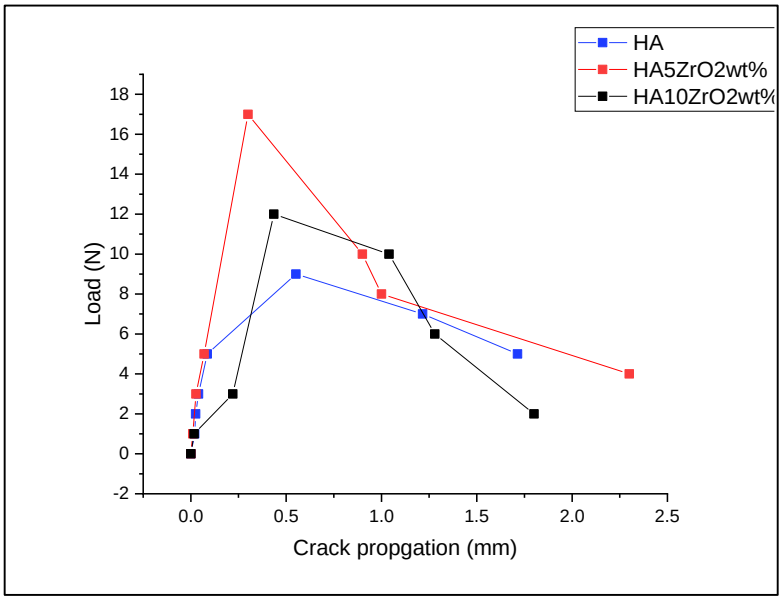

Figure (5.25) Load versus crack propagation.

5.5 Optimization Method

5.5.1 Regression Equation. A prediction model for physical properties (apparent porosity and density) and mechanical behaviour (fracture toughness) was established using the polynomial regression equation by taking these properties as a response (dependent variables) and the concentration of PSZ at the range between (0 – 20 wt. %) was taken as a continuous predictor (independent variables).

Polynomial regression was obtained by using the statistical program.

Polynomial regression for the density with PSZ content

$$\text{Density} = 2.728+0.1620(ZrO_2) -0.02614(ZrO_2)^2+0.000833(ZrO_2)^3 \quad (5.3)$$

The value of R-sq(91.27%)and R-(adj) (65.07%) .The analysis ANOVA is given in Table(5.1)

Table (5.1) Polynomial analysis Regression Equation of density

	Sum of squares	Df	Mean squares	F	Sig
Regression	0.568	3	0.189	3.483	0.371
Residual	0.054	1	0.054		
Total	0.622	4			

Polynomial regression for Porosity with PSZ content

Porosity = 9.786 - 2.398 (ZrO_2) + 0.4257(ZrO_2)² - 0.01267(ZrO_2)³ (5.4)

The value of R-sq(99%)and R-(adj) (98%) .The analysis ANOVA is given in Table(5.2).

Table (5.2) Polynomial analysis Regression Equation of porosity.

	Sum of Squares	Df	Mean Square	F	Sig
Regression	260.500	3	86.833	124.3	0.066
Residual	0.7	1	0.7		
Total	261.200	4			

Polynomial regression for Porosity with PSZ content

Pmax = 10.44 +4.993(ZrO_2) -0.6171(ZrO_2)² + 0.01800(ZrO_2)³ (5.5)

Where Pmax is critical Load. The value of R-sq(92.45%) R-(adj) (69.96%). The analysis ANOVA is given in Table(5.3)

Table (5.3) Polynomial analysis Regression Equation of Pmax.

	Sum of Squares	Df	Mean squares	F	Sig.
Regression	169.071	3	56.37	4.105	0.345
Residual	13.72	1	13.7		
Total	182.8	4			

Polynomial regression of the responses versus PSZ content is shown in Figure (5.25).

The R^2 value in the statistics is a key parameter. This is because, it indicates the model performance, depending on its value in each case, which is considered a good fit between the dependent and the independent variables.

5.5.2 Output Solution of GA

In this study, GA is applied using PSZ content in the range of (0wt. % - 20wt. %). The output of GA can be represented as a relation between the fitness value and several generations as illustrated in Figures (5.26), (5.27) and (5.28) for the density, apparent porosity and critical load .Table (5.4) illustrate the polynomial regression, best PSZ content, and optimum value for each property. The Optimum value result for the density is (3.01 g/cm^3) at (3.9) PSZ content, porosity is (6.05 %) at (3.3) PSZ, and critical Load is (22.249 N) at (5.1) PSZ content.

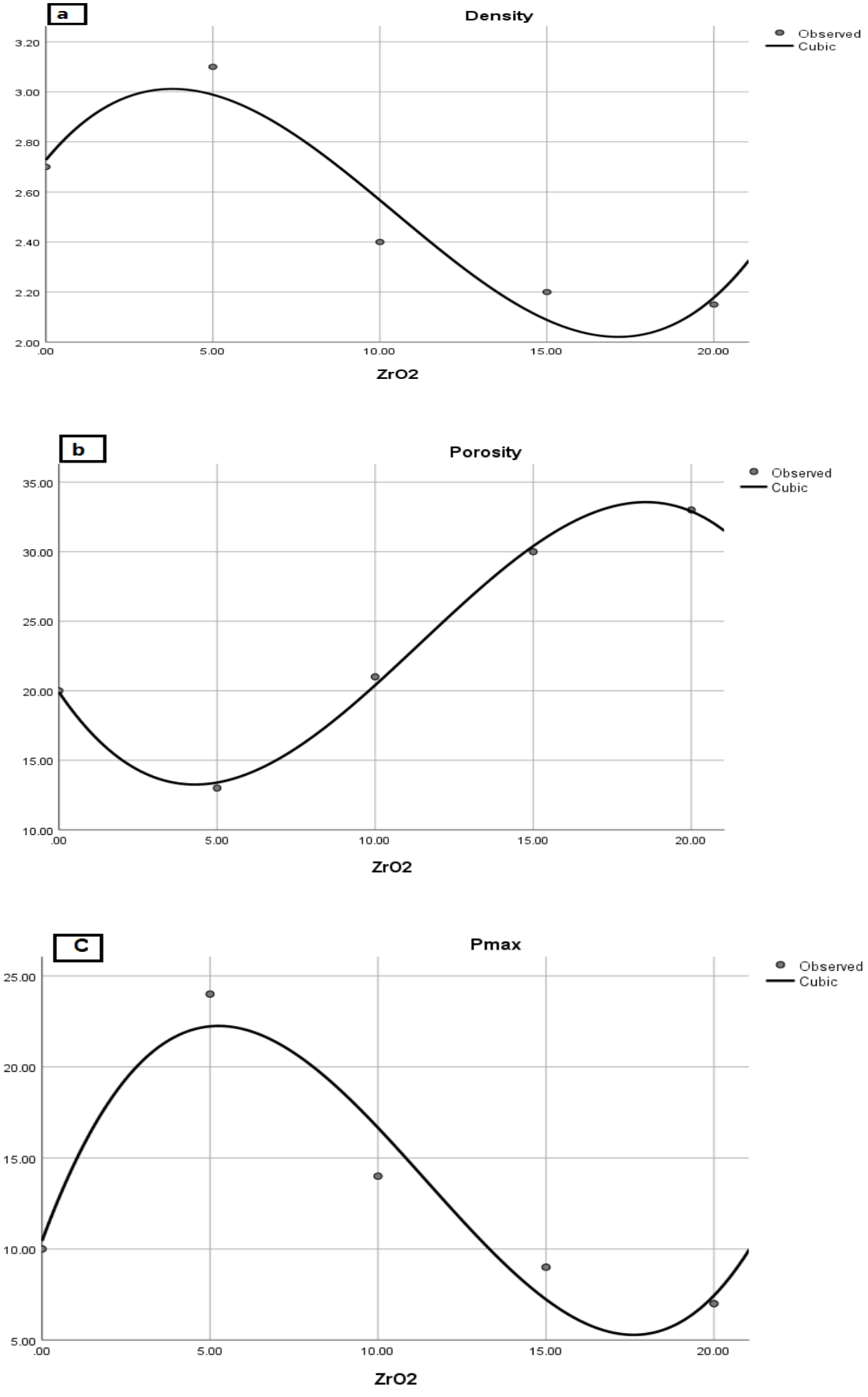

Figure (5.26) Polynomial Regression of PSZ Content versus a) Density, b) Porosity, c) Critical Load.

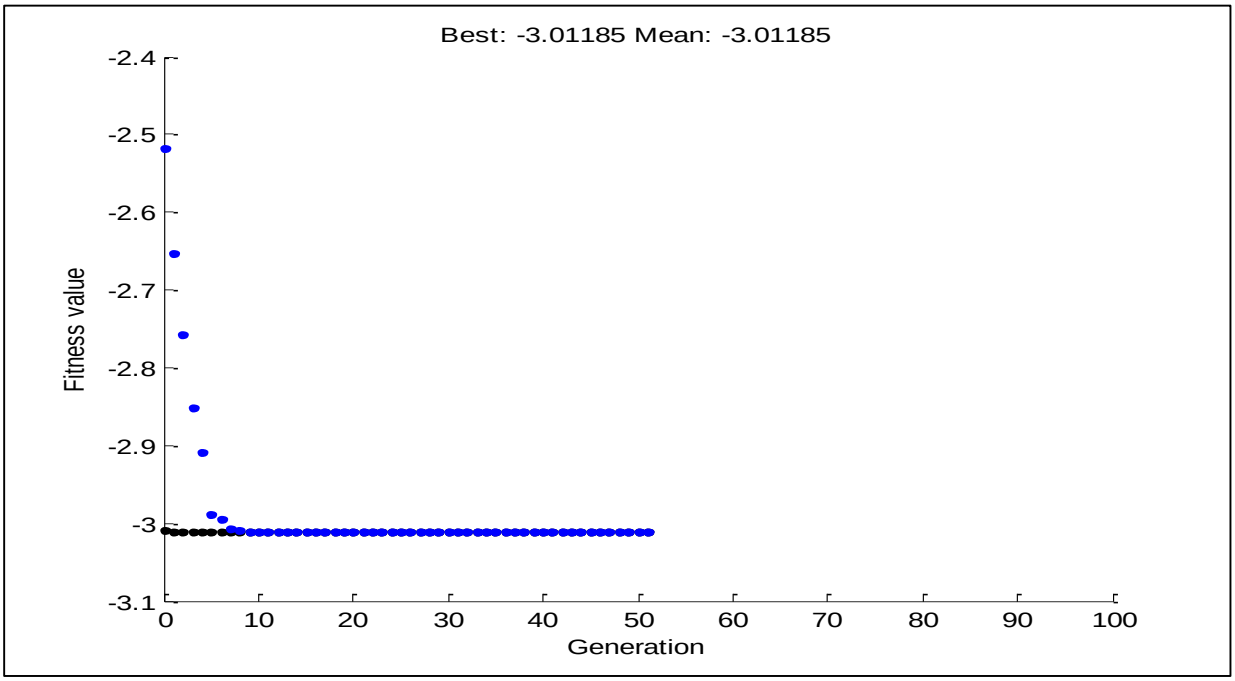

Figure (5.27) The generation versus the fitness value for density

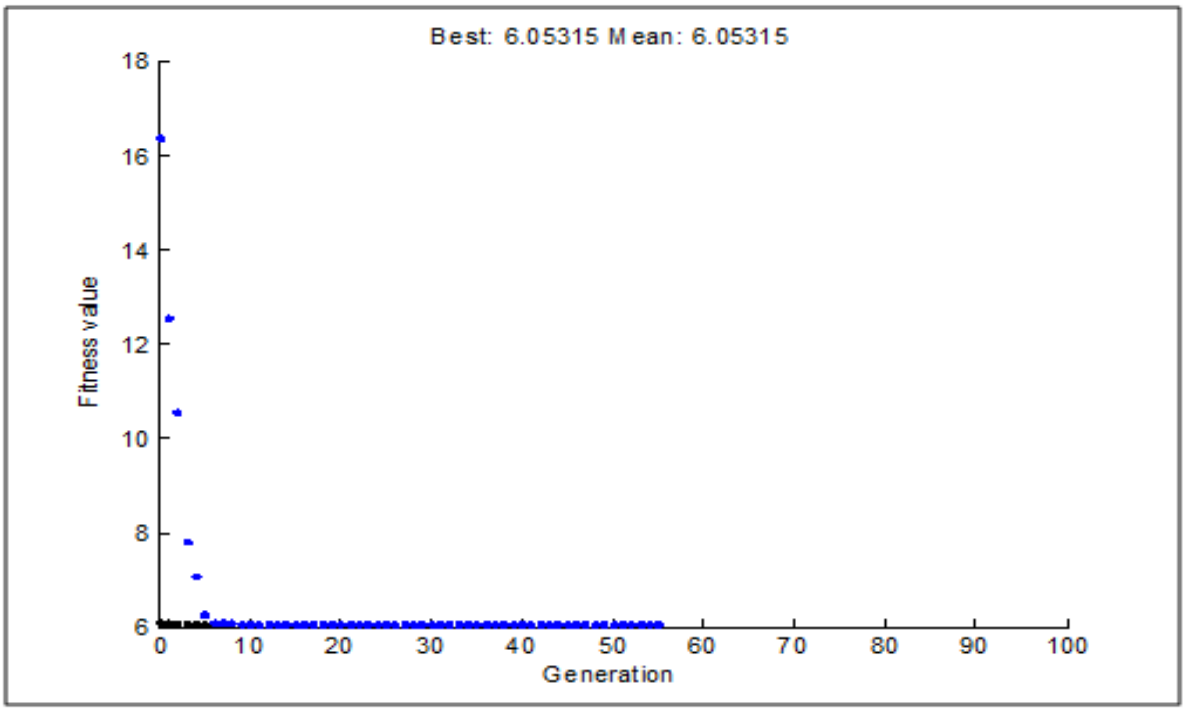

Figure (5.28) The generation verses the fitness value for porosity

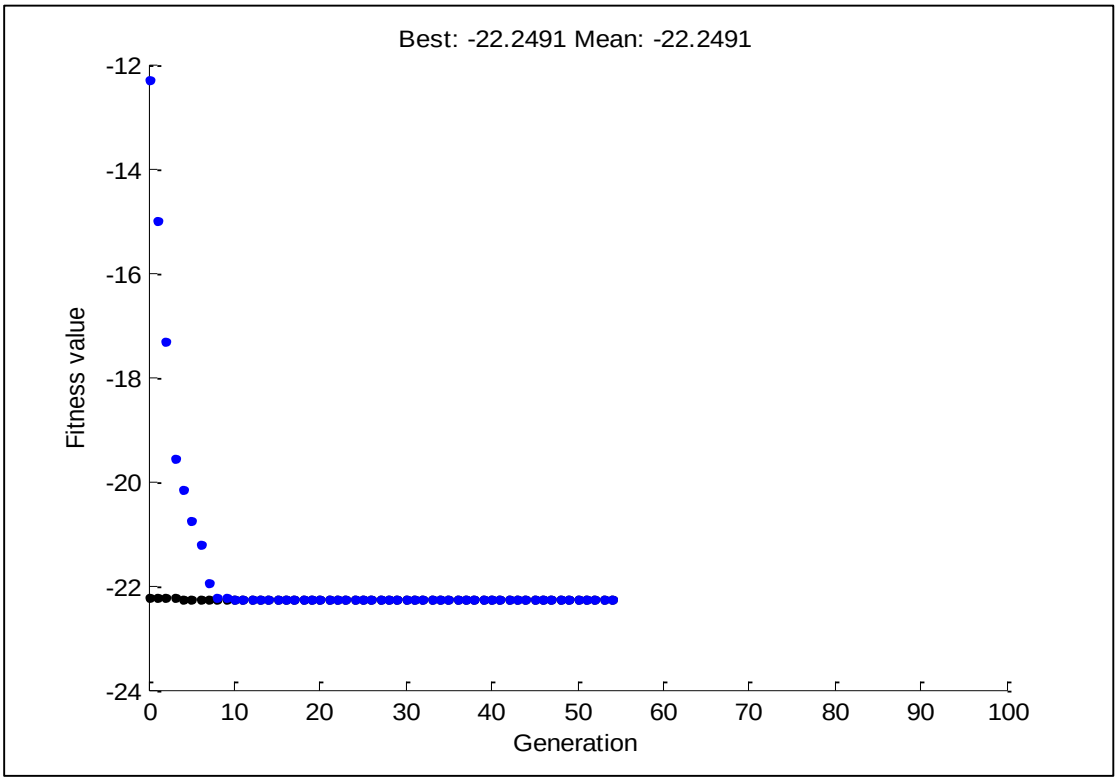

Figure (5.29) The generation versus the fitness value for critical Load

Table (5.4) Displays polynomial regression, best PSZ content and optimum property value for the dependent properties.

Property	Polynomial regression	Best PSZ	Optimum property
Density	Density = 2.728+0.1620(ZrO_2) – 0.02614(ZrO_2)²+0.000833(ZrO_2)³	3.9	3.011g/cm³
Porosity	Porosity =9.786 - 2.398 (ZrO_2) + 0.4257(ZrO_2)² - 0.01267(ZrO_2)³	3.3	6.05%
Critical load	Pmax = 10.44 +4.993(ZrO_2) - 0.6171(ZrO_2)²+ 0.01800(ZrO_2)³	5.1	22.249N

Chapter Six

Conclusions and Recommendations

6.1 Conclusion

According to the results of the experimental work and optimization method , can be concluded:

1. Extraction hydroxyapatite from Femur bovine bone is economical and safe method .
2. Hydroxyapatite can be toughened with partial stabilized zirconia but with ratio less than 10wt.% .
3. According to the results the best addition of zirconia concentrations was (HA/5wt.% ZrO_2) , Which improve the physical and the mechanical properties.
4. Critical loads of pure HA , HA/5wt.%ZrO_2 and HA/10wt.%ZrO_2 were 9 N ,17 N and 12 N.
5. DIC is appropriate technique to measure crack behavior (initiation and propagation of crack) for pure HA , HA/5%PSZ and HA/10%PSZ.
6. HA/15%PSZ and HA/20% PSZ was not controlled to measure initiation and propagation of crack due to its high brittleness.
7. CTOD for pure HA , HA/5wt.%ZrO_2 and HA/10wt.%ZrO_2 were 0.15 , 0.067 and 0.108 mm.
8. CMOD for pure HA , HA/5wt.%ZrO_2 and HA/10wt.%ZrO_2 were 0.196 ,0.091 and 0.193 mm.
9. Crack propagation for pure HA , HA/5wt.%ZrO_2 and HA/10wt.%ZrO_2 were 0.551 , 0.28 and 0.435 mm

10. Genetic algorithm method was suitable technique that used to give the optimum value of dependent variables (density , porosity and maximum load that sample bear it before failure) and independent variable (concentration of ZrO_2) .

6.2 Recommendations.

1. Use another method to prepare hydroxyapatite.
2. Study the effect of adding another materials like (Platinum, and PMMA) on the crack propagation and opening of hydroxyapatite.
3. Investigation crack propagation path and opening of hydroxyapatite by high resolution camera.
4. Investigation 2 D and 3 D crack of hydroxyapatite with digital image correlation.
5. Use strain age test to measure crack opening of hydroxyapatite .
6. Use numerical methods to measure crack propagation.

References

[1] S. M. Best, A. E. Porter, E. S. Thian, and J. Huang, “Bioceramics: past, present and for the future,” *J. Eur. Ceram. Soc.*, vol. 28, no. 7, pp. 1319–1327, 2008.

[2] A. Chetty, I. Wepener, M. K. Marei, Y. E. Kamary, and R. M. Moussa, “Synthesis, properties, and applications of hydroxyapatite,” Nova Science Publishers, 2012.

[3] A. Ruksudjarit, K. Pengpat, G. Rujijanagul, and T. Tunkasiri, “Synthesis and characterization of nanocrystalline hydroxyapatite from natural bovine bone,” *Curr. Appl. Phys.*, vol. 8, no. 3–4, pp. 270–272, 2008.

[4] A. Elghazel, R. Taktak, and J. Bouaziz, “Determination of elastic modulus, tensile strength and fracture toughness of bioceramics using the flattened Brazilian disc specimen: analytical and numerical results,” *Ceram. Int.*, vol. 41, no. 9, pp. 12340–12348, 2015.

[5] A. J. Ruys, M. Wei, C. C. Sorrell, M. R. Dickson, A. Brandwood, and B. K. Milthorpe, “Sintering effects on the strength of hydroxyapatite,” *Biomaterials*, vol. 16, no. 5, pp. 409–415, 1995.

[6] S. Asharaf, A. L. I. S. KARTHIGEYAN, M. Deivanai, and R. Mani, “Zirconia: properties and application" a review,” *Pakistan Oral Dent. J.*, vol. 34, no. 1, 2014.

[7] L. C. S. Nunes and J. M. L. Reis, “Estimation of crack-tip-opening displacement and crack extension of glass fiber reinforced polymer mortars using digital image correlation method,” *Mater. Des.*, vol. 33, pp. 248–253, 2012.

[8] J. J. Mecholsky Jr, “Fracture mechanics principles,” *Dent. Mater.*,

vol. 11, no. 2, pp. 111–112, 1995.

[9] T. Brynk, A. Laptiev, O. Tolochyn, and Z. Pakiela, “The method of fracture toughness measurement of brittle materials by means of high speed camera and DIC,” *Comput. Mater. Sci.*, vol. 64, pp. 221–224, 2012.

[10] Z. X. Lin, Z.-H. Xu, Y. H. An, and X. Li, “In situ observation of fracture behavior of canine cortical bone under bending,” *Mater. Sci. Eng. C*, vol. 62, pp. 361–367, 2016.

[11] W. Mekky and P. S. Nicholson, “The fracture toughness of Ni/Al2O3 laminates by digital image correlation I: Experimental crack opening displacement and R-curves,” *Eng. Fract. Mech.*, vol. 73, no. 5, pp. 571–582, 2006.

[12] T. Brynk, A. Laptiev, O. Tolochyn, and Z. Pakiela, “Digital Image Correlation Based Method of Crack Growth Rate and Fracture Toughness Measurements on Mini-Samples,” in *Key Engineering Materials*, 2014, vol. 586, pp. 96–99.

[13] G. M. Raghavendra, K. Varaprasad, and T. Jayaramudu, “Biomaterials: design, development and biomedical applications,” in *Nanotechnology applications for tissue engineering*, Elsevier, 2015, pp. 21–44.

[14] J. Park, *Bioceramics: properties, characterizations, and applications*, vol. 741. Springer Science & Business Media, 2009.

[15] M. Vallet-Regí, “Ceramics for medical applications,” *J. Chem. Soc. Dalt. Trans.*, no. 2, pp. 97–108, 2001.

[16] C. Palacio, D. Jaramillo, S. Correa, and M. Arroyave, “Study of the suitability of a commercial hydroxyapatite powder to obtain sintered

compacts for medical applications," in *Journal of Physics: Conference Series*, 2017, vol. 850, no. 1, p. 12021.

[17] A. A. Hendi, "Hydroxyapatite based nanocomposite ceramics," *J. Alloys Compd.*, vol. 712, pp. 147–151, 2017.

[18] C. B. Carter and M. G. Norton, "Ceramics in biology and medicine," *Ceram. Mater. Sci. Eng.*, pp. 635–651, 2007.

[19] G. Muralithran and S. Ramesh, "The effects of sintering temperature on the properties of hydroxyapatite," *Ceram. Int.*, vol. 26, no. 2, pp. 221–230, 2000.

[20] Y. Tanaka and K. Yamashita, "Fabrication processes for bioceramics," in *Bioceramics and their clinical applications*, Elsevier, 2008, pp. 28–52.

[21] S. Loher *et al.*, "Fluoro-apatite and calcium phosphate nanoparticles by flame synthesis," *Chem. Mater.*, vol. 17, no. 1, pp. 36–42, 2005.

[22] M. Askari Louyeh, "Silver, magnesium and zinc substituted hydroxyapatite for orthopaedic applications." University of Birmingham, 2017.

[23] E. M. Rivera-Muñoz and R. Fazel, "Biomedical Engineering—Frontiers and Challenges," 2011.

[24] M. Mucalo, *Hydroxyapatite (HAp) for biomedical applications*. Elsevier, 2015.

[25] N. Nagisa, T. Nakano, N. Hashiguchi, W. Fujitani, Y. Umakoshi, and M. Shimahara, "Analysis of biological apatite orientation in rat mandibles," *Oral Sci. Int.*, vol. 7, no. 1, pp. 19–25, 2010.

[26] M. Sadat-Shojai, M.-T. Khorasani, E. Dinpanah-Khoshdargi, and A.

Jamshidi, “Synthesis methods for nanosized hydroxyapatite with diverse structures,” *Acta Biomater.*, vol. 9, no. 8, pp. 7591–7621, 2013.

[27] H. Denissen, C. Mangano, and G. Venini, “Alveolar bone response to dense apatite ceramic implants in dogs,” in *Hydroxylapatite Implants*, Piccin Nuova Libraria SPA, Padua, 1985.

[28] N. A. S. M. Pu’ad, P. Koshy, H. Z. Abdullah, M. I. Idris, and T. C. Lee, “Syntheses of hydroxyapatite from natural sources,” *Heliyon*, vol. 5, no. 5, p. e01588, 2019.

[29] C. Piconi and G. Maccauro, “Zirconia as a ceramic biomaterial,” *Biomaterials*, vol. 20, no. 1, pp. 1–25, 1999.

[30] S. D. Bocanegra-Bernal, M. H., & De La Torre, “Phase transitions in zirconium dioxide and related materials for high performance engineering ceramics,” *J. Mater. Sci.*, vol. 37, no. 23, pp. 4947–4971, 2002.

[31] P. O. N. AGGLOMERATION, “www. globalscientificjournal. com,” *GSJ*, vol. 5, no. 8, p. 33, 2017.

[32] C. Viazzi, J.-P. Bonino, F. Ansart, and A. Barnabé, “Structural study of metastable tetragonal YSZ powders produced via a sol–gel route,” *J. Alloys Compd.*, vol. 452, no. 2, pp. 377–383, 2008.

[33] T. Liu, X. Zhang, X. Wang, J. Yu, and L. Li, “A review of zirconia-based solid electrolytes,” *Ionics (Kiel).*, vol. 22, no. 12, pp. 2249–2262, 2016.

[34] D. Roylance, “Introduction to fracture mechanics,” 2001.

[35] G. E. Dieter and D. J. Bacon, *Mechanical metallurgy*, vol. 3. McGraw-hill New York, 1986.

[36] L. B. Freund, “Dynamic Fracture Mechanics Cambridge University Press,” *New York*, 1990.

[37] J. Fineberg and M. Marder, “Instability in dynamic fracture,” *Phys. Rep.*, vol. 313, no. 1–2, pp. 1–108, 1999.

[38] A. A. Griffith, “VI. The phenomena of rupture and flow in solids,” *Philos. Trans. R. Soc. london. Ser. A, Contain. Pap. a Math. or Phys. character*, vol. 221, no. 582–593, pp. 163–198, 1921.

[39] B. Farahmand, “Linear elastic fracture mechanics (LEFM) and applications,” in *Fracture Mechanics of Metals, Composites, Welds, and Bolted Joints*, Springer, 2001, pp. 52–117.

[40] J. K. Wong, “Three-dimensional multi-scale hydraulic fracturing simulation in heterogeneous material using Dual Lattice Model.” University of Cambridge, 2018.

[41] M. F. Kanninen and C. L. Popelar, “Advanced fracture mechanics,” 1985.

[42] T. L. Anderson, *Fracture mechanics: fundamentals and applications*. CRC press, 2017.

[43] B. E. Jensen, “Numerical Analysis of Crack Propagation and Lifetime Estimation.” Esbjerg: Aalborg University, 2015.

[44] S. K. Maiti, *Fracture mechanics: fundamentals and applications*. Cambridge University Press, 2015.

[45] J. Pelleg, *Mechanical properties of ceramics*, vol. 213. Springer Science & Business, 2014.

[46] K.-J. Soderholm, “Review of the fracture toughness approach,” *Dent. Mater.*, vol. 26, no. 2, pp. e63–e77, 2010.

[47] G. V. G. REDDY and S. LJ, “Validation of the Methodology to Determine Stress Intensity Factor for a Axial Crack Emanating in a Pressurized cylinder.”

[48] S. Suresh, *Fatigue of materials*. Cambridge university press, 1998.

[49] M. Liu, Y. Gan, D. A. H. Hanaor, B. Liu, and C. Chen, “An improved semi-analytical solution for stress at round-tip notches,” *Eng. Fract. Mech.*, vol. 149, pp. 134–143, 2015.

[50] P. Kumar and K. Prashant, *Elements of fracture mechanics*. Tata McGraw-Hill Education, 2009.

[51] J. E. P. Ipiña, “CTOD for slow stable crack growth conditions,” *Fatigue Fract. Eng. Mater. Struct.*, vol. 15, no. 11, pp. 1091–1100, 1992.

[52] N. P. O’Dowd, “Fracture Mechanics: Nonlinear,” 2002.

[53] N. O’Dowd, “O.” Journal of Engineering Materials and Technology, p. 107, 2003.

[54] M. Rossi, “Crack propagation in brittle materials,” 2012.

[55] J. Kübler, “Fracture toughness of ceramics using the SEVNB method: preliminary results,” in *Proceedings of the 21st Annual Conference on Composites, Advanced Ceramics, Materials, and Structures—B: Ceramic Engineering and Science Proceedings*, 1997, vol. 18, pp. 155–162.

[56] A. Wang, P. Hu, X. Zhang, W. Han, G. Chen, and J. Han, “Accurate measurement of fracture toughness in structural ceramics,” *J. Eur. Ceram. Soc.*, vol. 37, no. 13, pp. 4207–4212, 2017.

[57] B. Basu and K. Balani, *Advanced structural ceramics*. John Wiley &

Sons, 2011.

[58] M. E. Launey and R. O. Ritchie, “On the fracture toughness of advanced materials,” *Adv. Mater.*, vol. 21, no. 20, pp. 2103–2110, 2009.

[59] M. V Swain, “Toughening mechanisms for ceramics,” in *Proceedings of The 7th International Conference On Fracture (ICF7)*, 1989, pp. 3739–3786.

[60] S. Erdem, “Synthesis and Characterization of Hydroxyapatite-Alumina-Zirconia Biocomposite,” *Master Sci. Diss. Grad. Sch. Eng. Sci. Izmir Inst. Technol.*, 2006.

[61] S. A. Meguid, “Mechanics and mechanisms of toughening of advanced ceramics,” *J. Mater. Process. Technol.*, vol. 56, no. 1–4, pp. 978–989, 1996.

[62] N. McCormick and J. Lord, “Digital image correlation,” *Mater. today*, vol. 13, no. 12, pp. 52–54, 2010.

[63] B. Pan, L. Yu, and D. Wu, “High-accuracy 2D digital image correlation measurements with bilateral telecentric lenses: error analysis and experimental verification,” *Exp. Mech.*, vol. 53, no. 9, pp. 1719–1733, 2013.

[64] S. Yoneyama and G. Murasawa, “Digital image correlation,” *Exp. Mech.*, vol. 207, 2009.

[65] S. P. Morgan, “An experimental and numerical study on the fracturing processes in Opalinus shale.” Massachusetts Institute of Technology, Department of Civil and Environmental …, 2015.

[66] M. Palanca, G. Tozzi, and L. Cristofolini, “The use of digital image correlation in the biomechanical area: a review,” *Int. Biomech.*, vol.

3, no. 1, pp. 1–21, 2016.

[67] I. Hilmi, M. Rinastiti, and M. K. Herliansyah, “Synthesis of hydroxyapatite from local bovine bones for biomedical application,” in *011 2nd International Conference on Instrumentation, Communications, Information Technology, and Biomedical Engineering2*, 2011, pp. 409–411.

[68] J. Manalu, B. Soegijono, and D. J. Indrani, “Characterization of hydroxyapatite derived from bovine bone,” *Asian J. Appl. Sci.*, vol. 3, no. 4, 2015.

[69] S. Sakakura and S. M. F. Pezzotti, GAsmus, “Hydroxyapatite toughened by silver inclusions,” *J. Compos. Mater.*, vol. 37, no. 23, pp. 2117–2129, 2003.

[70] R. E. Clegg and G. D. Paterson, “Ductile particle toughening of hydroxyapatite ceramics using platinum particles,” 2004.

[71] Z. E. Erkmen, Y. Genc, and F. N. Oktar, “Microstructural and mechanical properties of hydroxyapatite–zirconia composites,” *J. Am. Ceram. Soc.*, vol. 90, no. 9, pp. 2885–2892, 2007.

[72] C. H. Leong, A. Muchtar, C. Y. Tan, M. Razali, and N. F. Amat, “Sintering of hydroxyapatite/yttria stabilized zirconia nanocomposites under nitrogen gas for dental materials,” *Adv. Mater. Sci. Eng.*, vol. 2014, 2014.

[73] T. G. Aguirre, C. L. Cramer, V. P. Torres, T. J. Hammann, T. B. Holland, and K. Ma, “Effects of the addition of boron nitride nanoplate on the fracture toughness, flexural strength, and Weibull Distribution of hydroxyapatite composites prepared by spark plasma sintering,” *J. Mech. Behav. Biomed. Mater.*, vol. 93, pp. 105–117, 2019.

[74] J. Pittari and G. Subhash, “Fracture toughness testing of advanced silicon carbide ceramics using digital image correlation,” in *Dynamic Behavior of Materials, Volume 1*, Springer, 2015, pp. 207–212.

[75] A. J. Mohammed, M. Hussien, M. A. Aswad, and H. K. Rashed, “Investigation of crack propagation and opening in Hydroxyapatite using digital image correlation,” *J. Eng. Appl. Sci.*, vol. 12, no. 6, pp. 7935–7943, 2017.

[76] A. abd Selman, ―Study the effect of adding silver on the fracture mechanics of hydroxyapatite using digital image correlation.‖ 2019

[77] M. A. Aswad, I. K. Sabree, and A. H. S. Abd, “An examination of the effect of adding zirconia to bioactive glass-ceramic properties,” in *IOP Conference Series: Materials Science and Engineering*, 2021, vol. 1067, no. 1, p. 12121.

[78] A. P. D. S. Jaheel, “Optimize of the mechanical and physical properties of HA/B-TCP scaffold by using genetic algorithm method ”

[79] M. S. R. I. Abdalwahad and A. P. D. S. J. Edrees, “Preparation of Hydroxyapatite and Bioactive Glass Ceramic to Get Biocomposite by Using a Genetic Algorithm Method.”

[80] A. Chipperfield, P. Fleming, H. Pohlheim, and C. Fonseca, “Genetic algorithm toolbox for use with MATLAB,” 1994.

[81] S. Sangwan, “Literature Review on Genetic Algorithm,” *Int. J. Res.*, vol. 5, p. 1142, Jun. 2018.

[82] X.-S. Yang, *Engineering optimization: an introduction with metaheuristic applications*. John Wiley & Sons, 2010.

[83] M. Gen, R. Cheng, and L. Lin, *Network models and optimization:*

Multiobjective genetic algorithm approach. Springer Science & Business Media, 2008.

[84] P. Vas, *Artificial-intelligence-based electrical machines and drives: application of fuzzy, neural, fuzzy-neural, and genetic-algorithm-based techniques*, vol. 45. Oxford university press, 1999.

[85] S. Tiun, M. Ayob, M. A. AL-DhAlbadr, and F. Ief, "Genetic Algorithm Based on Natural Selection Theory for Optimization Problems," *Symmetry (Basel).*, vol. 12, no. 11, p. 1758, 2020.

[86] S. Mirjalili, "Genetic algorithm," in *Evolutionary algorithms and neural networks*, Springer, 2019, pp. 43–55.

[87] T. V Mathew, "Genetic algorithm," *Rep. Submitt. IIT Bombay*, 2012.

[88] C. R. Reeves, "Genetic algorithms," in *Handbook of metaheuristics*, Springer, 2010, pp. 109–139.

[89] E. E. E. Ali and E. Elamin, "A proposed genetic algorithm selection method," *King Saud Univ. Coll. Comput. Inf. Sci.*, 2006.

[90] A. Moonis, P. Chung, and C. Hinde, *Developments in Applied Artificial Intelligence: 16th International Conference on Industrial and Engineering Applications of Artificial Intelligence and Expert Systems, IEA/AIE 2003, Laughborough, UK, June 23-26, 2003, Proceedings*, vol. 2718. Springer, 2003.

[91] U. Mehboob, J. Qadir, S. Ali, and A. Vasilakos, "Genetic algorithms in wireless networking: techniques, applications, and issues," *Soft Comput.*, vol. 20, no. 6, pp. 2467–2501, 2016.

[92] S. S. Rao, *Engineering optimization: theory and practice*. John Wiley & Sons, 2019.

[93] L. Booker, “Improving search in genetic algorithms,” *Genet. algorithms simulated annealing*, pp. 61–73, 1987.

[94] H. A. Lafta and F. M. Salman, “Optimal path selection in ad hoc (MANET) by using genetic fuzzy petri net,” *Researcher*, vol. 6, no. 8, pp. 31–44, 2014.

[95] ASTM standards: C373-88, 1999. "standard test method for water absorption, bulk density, apparent porosity and apparent specific gravity of fired white ware products".

[96] ASTM C 1424-99, Standard Test Method for Compressive Strength of Advanced Ceramics at Ambient Temperature ics, 1999.

[97] A. International, *Standard test method for flexural strength of advanced ceramics at ambient temperature*. ASTM International, 2008.

[98] A. C. on C. on A. Ceramics, *Standard test methods for determination of fracture toughness of advanced ceramics at ambient temperature*. ASTM International, 2010.

[99] M. Mujahid, S. Sarfraz, and S. Amin, “On the formation of hydroxyapatite nano crystals prepared using cationic surfactant,” *Mater. Res.*, vol. 18, pp. 468–472, 2015.

[100] X.-J. Jin, “Martensitic transformation in zirconia containing ceramics and its applications,” *Curr. Opin. Solid State Mater. Sci.*, vol. 9, no. 6, pp. 313–318, 2005.

الخلاصة

تمت دراسة مادة الهيدروكسيباتيت نظرًا لتوافقها الحيوي الممتاز على نطاق واسع كمواد بديلة للعظام. يستخدم الهيدروكسيباتيت على نطاق واسع كمادة خزفية حيوية لزراعة الأنسجة الصلبة للإنسان لأنها تشبه تركيب العظام والأسنان إلى حد كبير. يقتصر استخدام الهيدروكسيباتيت على تطبيقات تحمل الأحمال المنخفضة نظرًا لخصائصه الميكانيكية الرديئة وخاصة متانة الكسر. في هذه الدراسة ، تم تحضير الهيدروكسيباتيت من عظم الفخذ البقري وذلك لكونه اقتصاديا وغير مضر للبيئة . وقد تم فحصه باستخدام حيود الأشعة السينية ، وتحليل حجم الحبيبي ، الأشعة تحت الحمراء.

تم تصنيع المادة المركبة من خلال استخدام مسحوق الهيدروكسيباتيت كمادة اساس ودقائق نانوية من مسحوق الزركونيا المثبتة جزئيا بنسب (0% , 5% , 10% ,20%) كمادة تقوية بطريقة ميتالورجيا المساحيق وذلك بكبس العينة تحت ضغط أحادي المحور ومُلبد عند 1250 درجة مئوية . بعد ذلك تم حساب الخواص الفيزيائية (بالكثافة والمسامية) والخواص الميكانيكية (مقاومة الانضغاط , صلادة فيكرز و مقاومة الانحناء) للمركبات.

تم استخدام اختبار الانحناء بثلاث نقاط وبحز مفرد لحساب سلوك الشق (نشوء الشق وتقدمه) وذلك عن طريق تقنية الارتباط الرقمي للصور والتي اعطت نتائج جيدة .

أظهرت النتائج التجريبية ان المركب (HA/5wt.ZrO_2%) له أعلى قيمة من ناحية الخواص الفيزيائية والميكانيكية عن النسب الأخرى ، حيث كانت الكثافة (3 جم / سم^3) مكعب ، مسامية (13٪) ، صلادة فيكرز(3.8 GPa) ، مقاومة الانضغاط (98 MPa) ، مقاومة الانحناء (43 MPa) ومتانة الكسر (1.1 MPa). كان تحول طور الزركونيا من طور رباعي الزوايا إلى طور أحادي الميل مسؤولاً عن آلية تقوية المركبات كنتيجة لوجود جزيئات الزركونيا التي عملت كعقبة أمام مقدمة الشق.

تم تطبيق طريقة الخوارزمية الجينية للحصول على أمثليه (الكثافة والمسامية واعلى حمل) وأفضل نسبة لأضافه دقائق مسحوق الزركونيا. أظهرت النتائج أن أفضل قيمة دالة للكثافة (3.01 جم / سم ³) عند (3.9 ٪ ZrO_2) ، أفضل قيمة دالة للمسامية (6.05٪) عند (3.3 ٪ ZrO_2). بالإضافة إلى أفضل قيمة دالة لأعلى حمل (22.2) عند (5.1 ٪ ZrO_2).

جمهورية العراق

وزارة التعليم العالي والبحث العملي

جامعة بابل

كلية هندسة المواد

قسم هندسة السيراميك ومواد البناء

أمثلية إضافة الزركونيا المثبتة جزئيا على متانة الكسر للهيدروكسيباتيت باستخدام الارتباط الرقمي للصور

رسالة

مقدمة الى كلية هندسة المواد / جامعة بابل وهي جزء من متطلبات نيل درجة الماجستير في هندسة المواد/ السيراميك

من قبل

مريم ابراهيم عريبي كاطع

إشراف

أ . د .
محسن عباس اسود الدجيلي

أ. د .
محمد عاصي احمد

1443ه

2022 م